ESCUELA POLITÉCNICA SUPERIOR DE MONDRAGON UNIBERTSITATEA
MONDRAGON UNIBERTSITATEKO GOI ESKOLA POLITEKNIKOA
MONDRAGON UNIVERSITY FACULTY OF ENGINEERING

Trabajo presentado para la obtención del título de
Titulua eskuratzeko lana
Final degree project for taking the degree of

GRADO EN INGENIERÍA BIOMÉDICA
BIOMEDIKAKO INGENIARITZA GRADUA
DEGREE IN BIOMEDICAL ENGINEERING

Título del Trabajo *Lanaren izenburua* Project Topic

STUDY THE CONTACT PERFORMANCE OF BIO-INSPIRED MECHANICAL JOINTS

Autor *Egilea* Author ALIONA SANZ IDIRIN

Curso *Ikasturtea* Year 2019/2020

Título del Trabajo *Lanaren izenburua* Project Topic

STUDY THE CONTACT PERFORMANCE OF BIO-INSPIRED MECHANICAL JOINTS

Nombre y apellidos del autor
Egilearen izen-abizenak
Author's name and surnames
SANZ IDIRIN, ALIONA

Nombre y apellidos del/los director/es del trabajo
Zuzendariaren/zuzendarien izen-abizenak
Project director's name and surnames
JEAN-MARC LINARES
ARRAZOLA, PEDRO JOSÉ

Lugar donde se realiza el trabajo
Lana egin deneko lekua
Company where the project is being developed
Aix Marseille Université

Curso académico
Ikasturtea
Academic year
2019/2020

Abstract (EN)

Mechanical joints tend to fail due to wear appearing caused by high localised loads. This work presents a new approach for the design of mechanical joints based on bioinspiration. Inspired in camel and bison geometry of the left elbow, mechanical joints were designed to analyse their load bearing performance. This work research numerically the influence of the morphology on the distribution of passing through mechanical loads. Different external loading conditions were tested by application of axial load, radial load and turnover moment in the mechanical joints. Contact pressure and areas were analysed by finite element method (FEM), and the influence of external loading on contact performance of the mechanical joints was discussed. Test results demonstrated that the morphology can significantly influence in load bearing performance. It was concluded that, camel-inspired mechanical joint has a better response to contact distribution between the shaft and the bearing, regarding to the bison-inspired mechanical joint, due to its shape characteristics. The preferential loading condition for each mechanical joint were found.

Keywords: load bearing performance, contact mechanics, bioinspiration, bio-inspired mechanical joints, finite element method (FEM)

Abstract (ES)

Las articulaciones mecánicas tienden a fallar debido al desgaste que aparece por las altas cargas localizadas. Este trabajo presenta un nuevo enfoque bioinspirado para el diseño de articulaciones mecánicas, diseñadas para analizar su rendimiento de carga inspiradas en la geometría del codo izquierdo del camello y el bisonte. Este trabajo investiga numéricamente la influencia de la morfología en la distribución de las cargas mecánicas que pasan a través de la articulación. Mediante la aplicación de carga axial, radial y momento de giro se probaron diferentes condiciones de carga externa en las articulaciones mecánicas. La presión y las áreas de contacto fueron analizadas mediante el método de elementos finitos (FEM), y se discutió la influencia de la carga externa en el rendimiento de contacto de las juntas mecánicas. Los resultados de las pruebas demostraron que la morfología puede influir significativamente en el rendimiento de la articulación. Se concluyó que la junta mecánica inspirada en el camello tiene una mejor respuesta a la distribución de contactos entre el eje y el rodamiento que la inspirada en el bisonte debido a sus características de forma. Se encontró la condición de carga preferencial para cada articulación mecánica.

Palabras clave: rendimiento de la carga, mecánica de contacto, bioinspiración, articulaciones mecánicas bioinspiradas, método de elementos finitos (FEM)

Abstract (EU)

Artikulazio mekanikoek huts egiteko joera dute higaduraren ondorioz agertzen diren karga lokalizatu altuengatik. Lan honek artikulazio mekanikoak diseinatzeko ikuspegi bioinspiratu berri bat aurkezten du. Artikulazio mekanikoak diseinatu ziren haien karga-errendimendua aztertzeko, gameluaren eta bisontearen ezkerreko ukondoaren geometrian inspiratuta. Lan honek morfologiak artikulazioan igarotzen diren karga mekanikoen banaketan duen eragina ikertzen du. Kanpoko karga-baldintza desberdinak probatu ziren artikulazio mekanikoetan karga axiala, erradiala eta biraketa-unea aplikatuz. Presioa eta kontaktu eremuak elementu finituen metodoaren bidez (FEM) aztertu ziren, eta kanpoko kargak artikulazio mekanikoen kontaktu errendimenduan zuen eragina eztabaidatu zen. Proben emaitzek erakutsi zuten morfologiak eragin nabarmena izan dezakeela artikulazioaren errendimenduan. Ondorioztatu zen, gameluan inspiratutako artikulazio mekanikoak erantzun hobea duela ardatzaren eta errodamenduaren arteko kontaktuen banaketan bisontean inspiratutakoarekin alderatuz gero dituen forma-ezaugarriengatik. Lehentasunezko karga-baldintza aurkitu zen artikulazio mekaniko bakoitzerako.

Hitz klabeak: kargaren errendimendua, ukipen-mekanika, bioinspirazioa, artikulazio mekaniko bioinspiratuak, elementu finituen metodoa (FEM)

Index

List of Figures

List of Tables

List of Abbreviations

AMU	Aix-Marseille Université
CBI	Bio Inspired Design (Conception bio-inspirée)
DOF	Degrees of Freedom
FEM	Finite Element Method
ISM	Institut des Sciences du Mouvement
MNHN	National Museum of Natural History
VBA	Visual Basic for Application
CJ*i*	Camel-inspired joint N°*i*
BJ*i*	Bison-inspired joint N°*i*
BH	Bison humerus
CR	Camel radius
BR	Bison radius
CS	Camel shaft
BS	Bison shaft
CB	Camel bearing
BB	Bison bearing

List of Symbols

E	MPa	Young's modulus
v		Poisson's ratio
F_a	kN	Axial force
F_r	kN	Radial force
M_t	Nm	Turnover moment
$\mathrm{P_{max}}$	MPa	Peak contact pressure
$\overline{\mathrm{P_{max}}}$	MPa	Average peak contact pressure

Chapter 1. Introduction

One of the main objectives of this work is to understand how biological joints operate in Nature in order to bio-inspire the design of mechanical joints. In this chapter is presented a brief summary of the work carried out during this project. This chapter includes aspects concerning the background of this project, state of the art that include the previous work and voids of performed studies, objectives, phases and specific conditions of the project. In the state-of-the-art biological joints types, the importance of a proper performance of mechanical joints and problems with their lifespan are analysed.

1.1. Synopsis

Joints are connections between two or more parts of a multibody systems that are present in both natural and man-made systems. Their example can be seen in exoskeletons, endoskeletons, helicopters and robotic arms, for instance. An asymmetric or unbalanced load transmission generates premature wear in the joint decreasing its lifespan. In the medical and industrial fields, efforts of the scientific community are mainly focused on improving joints lifespan.

Evolution capacity of species has allowed them to adapt to the surrounding environment and survive over the years. This evolution has introduced improvements in several aspects such as physiologic and anatomic, allowing biological systems to develop specialized subsystems (sensor, locomotor, control, skeletal, muscular) very elaborated and with better characteristics than artificial systems.

Through bioinspiration, inspiration in biological processes and structures, evolutionary improvements are used to solve problems from different fields. Considering this, the opportunity to use the biological joint morphologies as inspiration source in engineering design has been found. The aim of the present study was to evaluate the load bearing performance advantages of the two morphologies proposed by Nature for the hinge joint.

For the development of this project left elbow bone samples obtained from species received from the National Museum of Natural History in Paris (*Camelus bactrianus* MNHN-ZM-AE-2007-1435 and *Bison bison* MNHN-ZM-AC-1951-242) have been used. The reason to use elbow joints is because they are the most similar to industrial kinematic joints. This type of joint allow rotation around one axis like human hinge joints (flexion-extension movement), but unlike them, they do not allow rotation (pronation-supination movement). Above, the size of these elbows and weight of these animals are comparable, which make a feasible comparison.

Las articulaciones son las conexiones entre dos o más partes de un sistema multicuerpo que están presentes tanto en los sistemas naturales como en los artificiales. Su ejemplo puede verse en los exoesqueletos, endoesqueletos, helicópteros y brazos robóticos, por ejemplo. Una transmisión de carga asimétrica o desequilibrada genera un desgaste prematuro de las articulaciones disminuyendo su vida útil. En los ámbitos médico e industrial, los esfuerzos de la comunidad científica se centran principalmente en mejorar la vida útil de las articulaciones.

Debido a la capacidad de evolución de las especies, estas han podido adaptarse al entorno que les rodea y así sobrevivir a lo largo de los años. Esta evolución ha introducido mejoras en varios aspectos como en la fisiología y en la anatomía, permitiendo así que las estructuras biológicas desarrollen subsistemas especializados (sensorial, locomotor, control, esquelético, muscular) muy elaborados y de mejores características que los sistemas artificiales.

Mediante la bio-inspiración, la inspiración en procesos y estructuras biológicas, se intenta aprovechar las mejoras evolutivas para dar solución a problemas de distintos campos. Teniendo esto en cuenta, se ha encontrado la oportunidad de utilizar las distintas morfologías de articulaciones biológicas como fuente de inspiración en el diseño de ingeniería. El objetivo de este estudio ha sido evaluar las ventajas de rendimiento de carga de las dos morfologías propuestas por la naturaleza para la articulación de bisagra.

Para el desarrollo de este proyecto se han utilizado muestras de huesos de las articulaciones del codo izquierdo que se obtuvieron de especies recibidas del Museo Nacional de Historia Natural de París (*Camelus bactrianus* MNHN-ZM-AE-2007-1435 and *Bison bison* MNHN-ZM-AC-1951-242). La razón de utilizar articulaciones de codo es porque son las más parecidas a las articulaciones cinemáticas industriales. Este tipo de articulaciones permiten la rotación alrededor de un solo eje, como las articulaciones humanas de bisagra (movimiento de flexión-extensión), pero a su diferencia, no permiten el movimiento rotacional (pronación-supinación). Además, las dimensiones de los codos y el peso de estos animales son comparables, lo cual hace la comparación más factible.

Giltzadurak sistema multigorputz baten bi zati edo gehiagoren arteko konexioak dira, sistema naturaletan zein artifizialetan agertzen direnak. Hauen adibidea exoeskeletoetan, endoeskeletoetan, helikopteroetan eta beso robotikoetan ikus daiteke. Karga asimetrikoa edo desorekatua transmititzeak giltzaduren higadura goiztiarra eragiten du, eta bizitza erabilgarria murrizten du. Arlo medikoan eta industrialean komunitate zientifikoak ahaleginak giltzaduren bizitza erabilgarria luzetzean datzate.

Espezien eboluzio gaitasuna dela eta, hauek ingurunera egokitu ahal izan dira, eta horrela, urteetan zehar biziraun ahal izan dute. Bilakaera horrek hobekuntzak ekarri ditu hainbat alderditan, hala nola fisiologian eta anatomian. Horrela, egitura biologikoek azpisistema espezializatuak garatu ahal izan dituzte (sentsoriala, lokomotorea, kontrola, eskeletikoa, muskularra), oso landuak eta sistema artifizialek baino ezaugarri hobeagoak dituztenak.

Bioinspirazioaren bitartez, prozesu eta egitura biologikoetan inspiratuz, eboluzio-hobekuntzak beste arlokuntzetako arazoei irtenbidea emateko erabiltzen dira. Hau kontuan hartuta, artikulazio biologikoen morfologiak ingeniaritzaren diseinuan inspirazio-iturri gisa erabiltzeko aukera aurkitu da. Ikerketa honen helburua naturak banda-giltzadurentzako proposatutako bi morfologien karga-errendimenduaren abantailak ebaluatzea izan zen.

Proiektu hau garatzeko, Parisko Historia Naturaleko Museo Nazionalak (*Camelus bactrianus* MNHN-ZM-AE-2007-1435 and *Bison bison* MNHN-ZM-AC-1951-242) eskainitako ezkerreko ukondoaren giltzaduraren hezur-laginak erabili dira. Ukondoko artikulazioa erabiltzearen arrazoia giltzadura zinematiko industrialen antzekoenak direlako da. Mota honetako artikulazioek ardatz bakar baten inguruan biratzea ahalbidetzen dute, giza banda-giltzadurak bezala (flexio-hedadura mugimendua), aldiz, ez dute pronazio-supinazio mugimendua ahalbidetzen. Gainera, ukondoen neurriak eta animalia horien pisua konparagarriak dira, eta horrek konparazioa egingarriagoa egiten du.

1.2. Previous work

This project has been carried out in the research team Bio Inspired Design (CBI) which corresponds to the *Institut des Sciences du Mouvement* (ISM – UMR 7287) of *Aix-Marseille Université* (AMU).

AMU is composed by different institutes, which are grouped by different themes. One of the institutes is the ISM and their goal is to study the mechanical, physiological, neurological, psychological and sociological determinants of the motricity of living beings. ISM as of today is formed by nine different research teams, CBI being part of them. CBI team seeks to know how Nature has realized limited-motion kinematic connections/joints and how to inspire them to propose new artificial links for industrial mechanisms.

Some of recent publications in relation to natural joint from a biomechanical point of view of the CBI team are:

- "A multivariate statistical strategy to adjust musculoskeletal models" published in journal of Biomechanics [1].
- "Effects of realistic sheep elbow kinematics in inverse dynamic simulation" published in PLOS ONE journal [2].
- "Joint loading estimation method for horse forelimb high jerk locomotion: jumping was performed", published in Journal of Bionic Engineering [3].

In the last year, CBI team has been interested in the analysis of the contact mechanics performance of different elbows morphologies that exist in Nature. The purpose of this research line is to understand how joints morphology influence on passing through mechanical load distribution and what has led them to behave the way they do. In addition, by analysing these answers find sources of bioinspiration for the design of the mechanical joints.

CBI team analysed that in some cases, Nature has created different morphologies for the same kinematic requirements (same DOF). An example of this case is the hinge elbow joint (one DOF in rotation). In some quadrupedal mammals, their elbow is formed by a two well defined condyles (trochlea and capitellum) (hereafter called morphology I or two bumps morphology) (see left-hand side of Figure 1.1). Some animals presenting this characteristic can be seen on the left-hand side of Figure 1.2. However, a different elbow morphology can be found in other quadrupedal mammals. The elbow of these animals presents a capitellotrochlear sulcus between the capitellum and the trochlea (hereafter called morphology II or three bumps morphology) (see right-hand side of Figure 1.1). Some animals presenting this characteristic can be seen on the right-hand side of Figure 1.2.

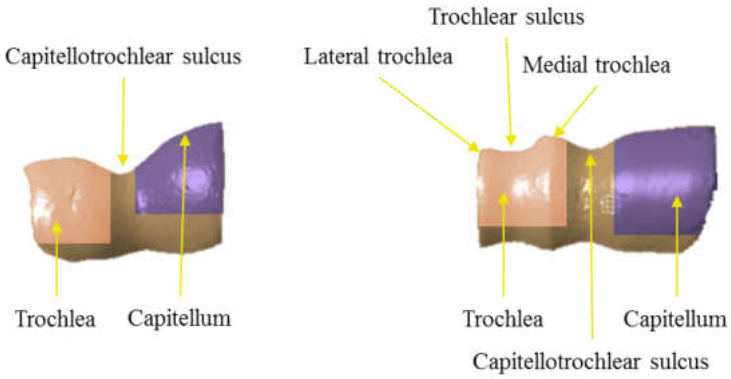

Figure 1.1: Morphologies explanation.

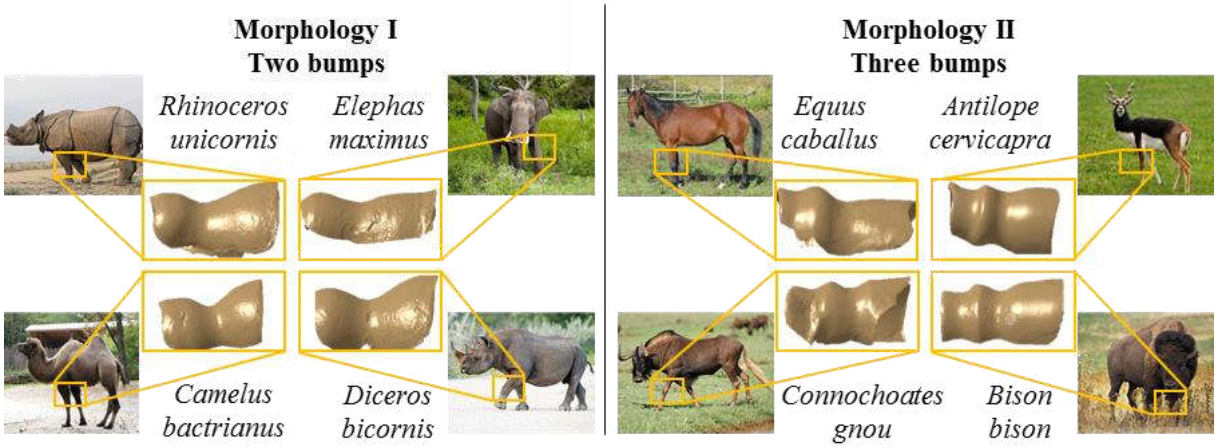

Figure 1.2: Animals classification according their elbow morphology accompanied by 3D surface model of the distal humerus articulation. On the left side, group of animals with two bumps and on the right side, group of animals with three bumps. [4]

These species were provided by National Museum of Natural History in Paris and their collection reference numbers are indicated in Table 1.1. To the best knowledge of the author, no interpretation has been proposed to the coexistence these morphologies. Neither the relationship of morphology with the load bearing performance has been studied jet. A better understanding of the coexistence of these morphologies and their functional advantages can provide new insights to improve the design of current mechanical joints. With these interests in mind the project presented throughout this document was carried out.

Table 1.1: Collection reference number of the scanned bones from the National Museum of Natural History in Paris.

Species	**Reference to the collection of National Museum of Natural History in Paris**
Antilope cervicapra	MNHN-ZM-AC-1888-734
Bison bison	MNHN-ZM-AC-1951-242
Connochoates gnou	MNHN-ZM-AC-1976-344
Diceros bicornis	MNHN-ZM-AC-1944-278
Equus caballus	MNHN-ZM-AC-1932-46
Rhinoceros unicornis	MNHN-ZM-AC-1885-734
Camelus bactrianus	MNHN-ZM-AE-2007-1435
Elephas maximus	MNHN-ZM-1896-17

1.3. State of the art

Joints are the connections between two or more parts of a multibody systems that are present in both natural and man-made systems. Natural systems often exploit intricate multiscale and multiphase structures and consequently they are able to achieve superior functionalities to those of artificial systems [5]. State of the art information was focused on scientific works of both biological and mechanical joints.

Among the analysed bibliography, most of the researches about mechanical joints are focused on failure preventing and increasing their lifespan. With the aim of improving the performance of current industrial mechanical joints the research team CBI seeks to innovate using bioinspiration. The knowledge provided by bioinspiration has already been integrate into several sectors, such as robotics, chemistry, aeronautics, architecture and many more.

To be able to apply bioinspiration in different areas first is important to understand its operating principle using biomechanics. With the purpose of using this information for the design of bio-inspired mechanicals joints, a state of the art has been done to analyse different types of biological joints, how they work and understand their structural and mechanical

behaviour. The aggrupation of the analysed bibliography can be seen in Figure 1.3. Joints are grouped into two main categories biological or mechanical. First, biological joints types are analysed. Analysed studies performed with biological joints are grouped into two different lines of research: ones for medical purposes and second group with phylogenetic purposes. Second, studies related to mechanical elements (bearings) performance are presented.

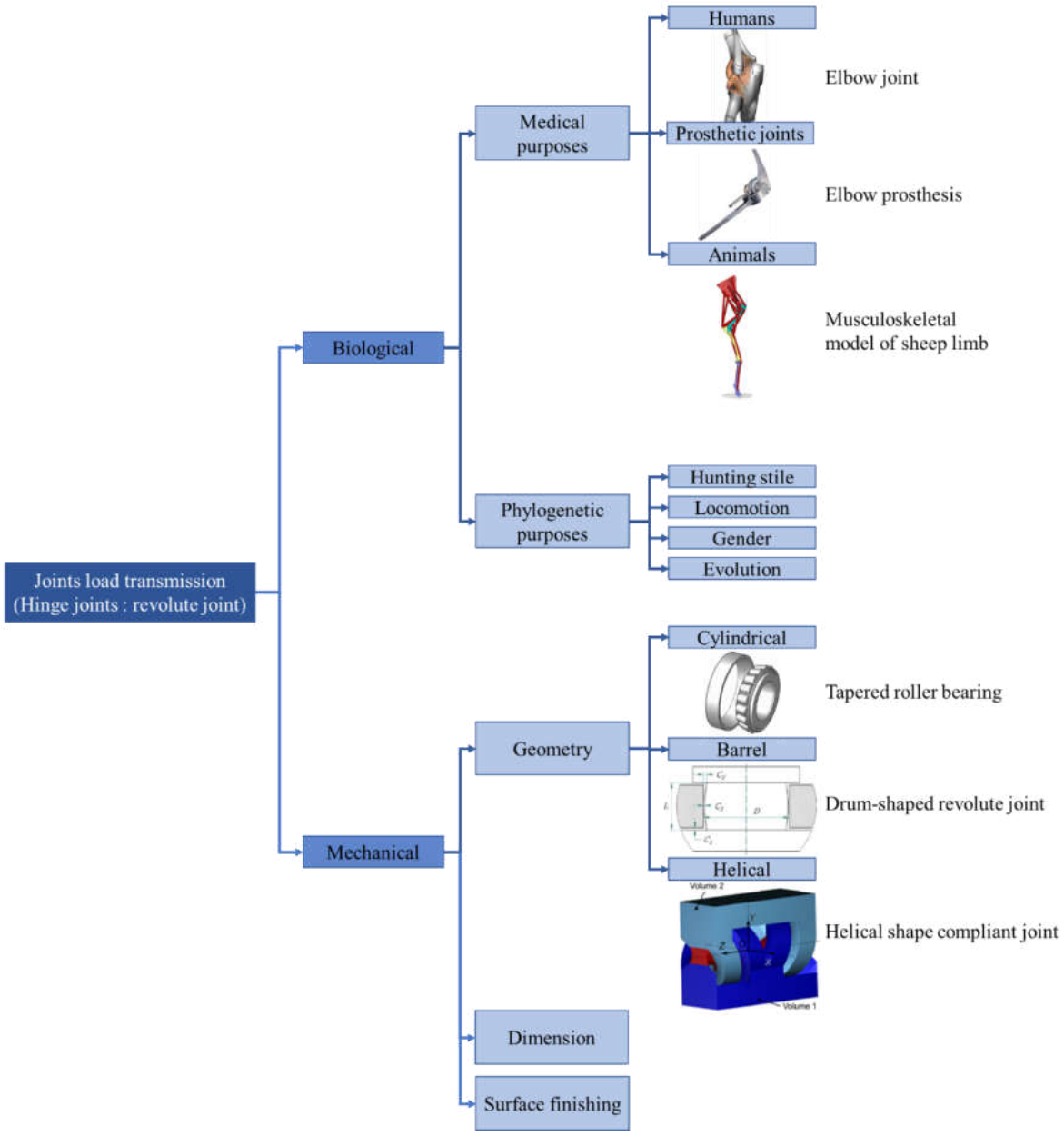

Figure 1.3: Literature review. [2], [4], [6], [7]

1.3.1. Biological joints

In biological systems, the contact point between a bone and cartilage, bone or teeth is called as joint [8]. Joint is formed when two bone articulate with each other. Joints

categorisation can be on their anatomical attributes (structurally) or according the movement they allow (functionally). In Figure 1.4 can be seen the aggrupation of the biological joints described below.

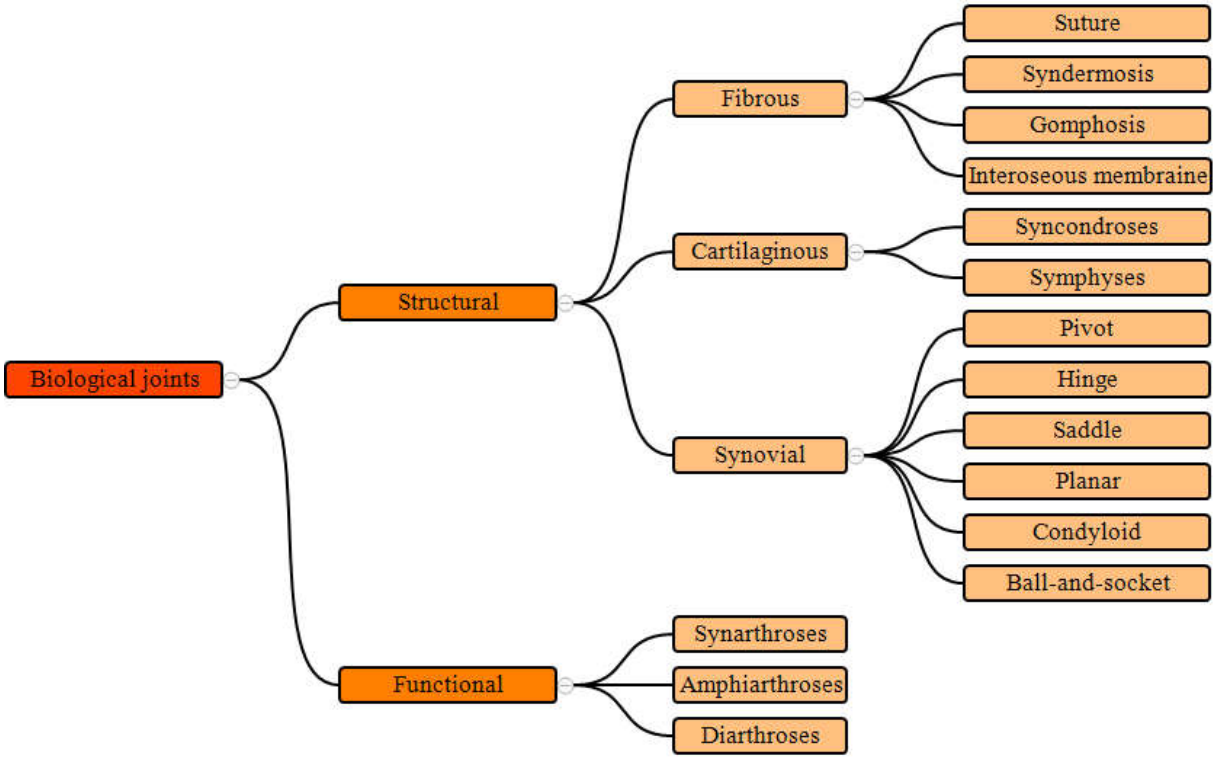

Figure 1.4: Biological joints aggrupation.

The presence or absence of the synovial cavity (a space between the articulating bones) and type of the connective tissues that bind the bones together determine joints' structural classification. During this aggrupation three type of joints are identified: fibrous joints, cartilaginous joints and synovial joints.

Fibrous joint. These joints are described by absence of synovial cavity between bones and dense irregular connective tissue held them together. They do not permit any movement or little. Fibrous joints examples can be seen in skull called sutures, syndesmosis between radioulnar and tibiofibular joints, gomphosis between tooth and socket, and interosseous membranes between diaphysis of neighbouring long bones as tibia-fibula or radius-ulna (see Figure 1.5).

Cartilaginous joint. These joints do not have synovial cavity and have reduced degrees of movement to null or little. Hyaline cartilage or fibrocartilage tightly connect the articulating bones. Two types of cartilaginous joints can be identified: synchondroses (joins the epiphysis to the diaphysis in growing long bone) and symphyses (permanent joint in the midline of the

body, as for example pubic, sternum and intervertebral symphysis). Example of this type of joints can be seen in Figure 1.5.

Synovial joint. The articulating bones of this type of joints present synovial cavity between them. This cavity allows joints movement, so functionally they are considered as diarthroses, free movable joints. Hyaline cartilage layer covers the bones, without binding them, reducing friction and absorbing the shock. This type of joint is characterized by a wide variety of shapes and different types of movement.

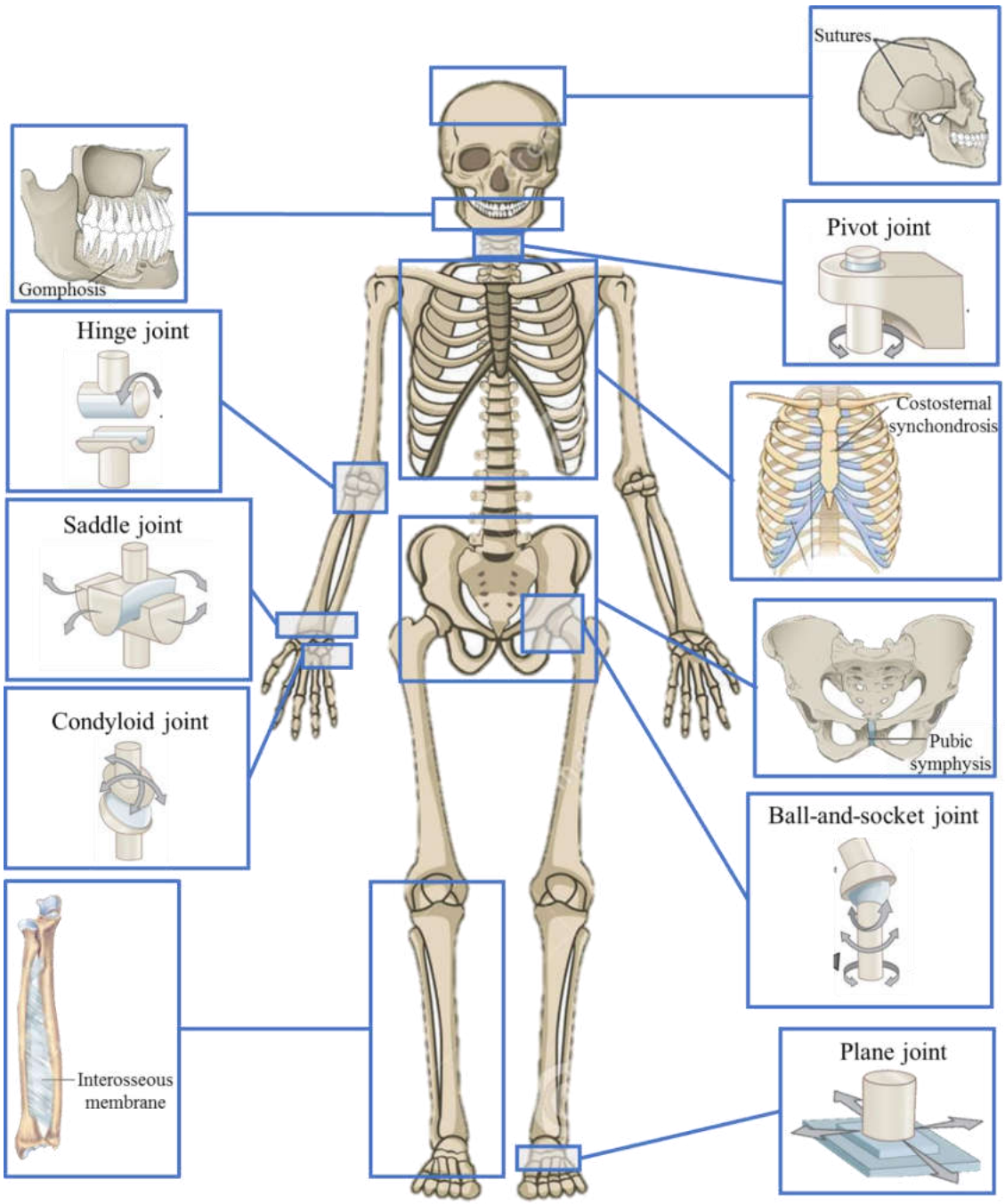

Figure 1.5: Different joint types. [4]

Joints degrees of movement determine their functional category. During this categorization three type of joints are identified: synarthroses (fixed joints), amphiarthroses (hardly movable joints) and diarthroses (freely movable joints).

The focus of this study is on synovial joints due to the degrees of movement that they allow. These joints are the ones that most resemble to the industrial kinematic joints. Following the allowed degrees of freedom (DOF) in different freely movable joints are analysed.

Pivot joint. These joints articulate between rounded or pointed surface of one bone with a bone and ligament ring. The only movement of these joints is rotation around their longitudinal axis. Examples of this joint are between C1 and C2 vertebrae and radioulnar joint.

Hinge joint. These joints consist of two bones that fit together, one with a convex surface and the other with a concave surface. Angular movement around one axe, opening-and-closing, is the movement that they perform. Examples of this joint are elbow, hand phalanges, knee, ankle and toes.

Saddle joint. In these joints, joint articular surfaces of two bones fit together through the saddle-shape of one of them. Biaxial movement is permitted by these joints. Examples of this joint are chest sternoclavicular joint and carpometacarpal joint

Planar joint. The bones of these type of joints are distinguished by flat or slightly curved surfaces. Primarily they move side-to-side and backward-and-forward, but they also may rotate one against the other. Example of this joint can be seen between tarsal bones.

Condyloid joint. In these joints two bones fit together through a convex oval surface of one bone and concave oval cavity of another one. They allow biaxial movement, around two axes, the same as in saddle joints. Example of this joint is wrist joint.

Ball-and-socket joint. These joints consist of a bone that end in a ball surface and fit into a cup form cavity of another bone. These joints are triaxial, as the allow the movement around three axes.

As mentioned before, analysed studies performed with biological hinge joints can be grouped into two different lines of research: ones for medical purposes and second group with phylogenetic purposes.

(a) Medical studies

On the one hand, studies for medical purposes determine load transmission and biomechanics of the joints. These studies have been performed in elbow [9], [10], finger [11], knee [12]–[16] and ankle [16] joints. An asymmetric or unbalanced load transmission in biological joints can lead to increased stress in the joint, developing cartilage wearing [17], [18]. This wear can cause osteoarthritis, which in worst case may require a surgery, with partial removing of the joint or replacement by prosthesis [19].

Acquired knowledge from the performed studies with biological joints are later used for the improving the design of prosthetic joints increasing their lifetime and reducing patients' pains [3]. The aforementioned studies helped for the design and the development of prostheses for knee [20]–[22], ankle [23] and elbow [24], [25] joints. Among the studies carried out for medical purposes, only physiological loading conditions were analysed. Therefore, a gap has been found in the research on the technological advantages of these joints for their subsequent use as a source of bioinspiration.

(b) Phylogenetic studies

On the other hand, studies with phylogenetic purposes are centred in the evolution of species classifying animals according their similarities and differences. These kind of studies analyses the shape of distal humerus joint in order to relate its morphology with the hunting style of the animal, locomotion or to estimate forelimb posture in extinct quadruped animals [26]–[28]. Also, a study to analyse the difference of elbow joint morphologies between different species and sexes was performed. In this study they concluded that larger animals have larger joints but no relation found about sex influence on elbow morphology of the same species [29].

In some cases, Nature has created different morphologies for the same application with the same DOF. An example of this case is the hinge elbow joint (one DOF in rotation). In some quadrupedal mammals, the articular surface of the elbow joint present a revolution profile characterized by two bumps while others present three bumps.

Despite all these evolutive studies with different morphologies, no interpretation has been proposed to the coexistence these morphologies. Neither the relationship of morphology with the load bearing performance has not been studied jet. A better understanding of the coexistence of these morphologies and their functional advantages can provide new insights to improve the design of current mechanical joints.

1.3.2. Mechanical elements

Kinematic joints are the connection between two or more independent parts of a multibody system. Mechanical joints are common points of failure of mechanical systems and structures. Cylindrical joints are the technological equivalent of biological hinge joints. Their reliability is therefore of vital importance in technological development especially in aerospace engineering. In a context of energetic transmission and eco-design, design more reliable and efficient systems is a priority.

In the industrial field, studies have been performed about tribological performance to analyse the mechanical efficiency of the mechanical elements (roller bearing and sliding bearings, Figure 1.6). In contrast with rolling bearings, sliding bearings support higher loads and work at lower speeds. These studies seek to extend bearings lifetime, maximize their load bearing performance and reduce premature wear appearing. During these studies the optimal surface finishing [30]–[33], dimensions [34]–[40] and clearance [41], [42] of the bearings were defined.

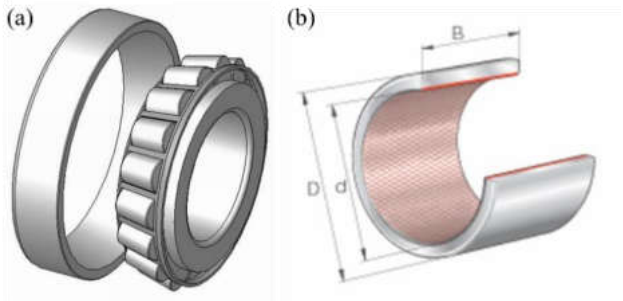

Figure 1.6: (a) Tapered roller bearing and (b) sliding contact bearing. [Extracted from ABF enterprise]

Current design of bearings is based on simple geometries and might present angular misalignments during operation (Figure 1.7) [43]. This, in turn, generates high contact pressures and hence an accelerated surface wear [44]–[47]. Despite the improvements in materials science and lubricating systems these issues are persistent affecting the system reliability and its energetic efficiency. So as to solve the problem of premature failure, failure prediction researches and methodologies have been developed [48]–[50]. They designed different algorithms monitoring data, while application, and predicted lifetime.

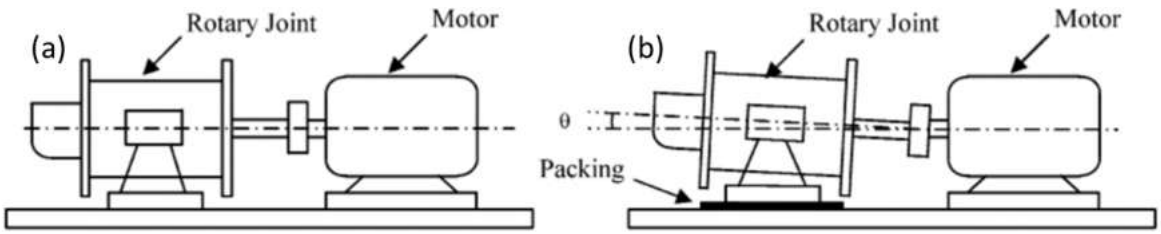

Figure 1.7: Shafts in (a) aligned condition and (b) misaligned condition. [43]

Reduced number of studies exist about non-cylindrical geometry bearings. Non-cylindrical geometries could help to prevent premature wear appearing due to misalignment. New designs for revolute joint have been explored by Wei et al [6] and Bruyas et al [7]. They performed tension and extension tests and demonstrated that is possible to manufacture joints with geometries other than cylindrical and that their performance could be better compared to the conventional ones. However, their studies have limitations since they need more dynamic analysis, as depending on the design the friction forces will dominate the inertial forces limiting the application and enhance the compliant between the parts in order to ensure their performances. In Figure 1.8 can be seen an example of a joint with different geometry to the common bearings.

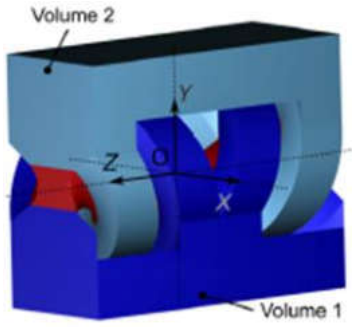

Figure 1.8: Helical shape compliant joint. [7]

Nowadays the industry keeps designing and manufacturing simple geometry bearings. In fact, bearings geometry has not developed in several decades even if the new technologies, additive manufacturing or 5-axes CNC machining, allow to create more complex and efficient pieces than before. The consequences of stagnation in the development of industrial components can be seen in the premature failure of several components as seals and bearings. [43], [51]

The lack of non-cylindrical geometry component might be due to easy manufacturing of the cylindric ones. Nevertheless, manufacturing technologies of nowadays allow to perform complex geometries by additive manufacturing or 5-axes CNC machining. So technological barriers have been knocked down opening the way for development of new design paradigms, as can be the bioinspiration.

Biological systems tend to perform better than artificial ones. Bioinspiration is a method of taking advantage of these characteristics of biological systems and translating them into mechanical application. Bioinspiration studies have been already performed in several fields as for example robotics to improve locomotion aspects [52]–[56] or in mechanics structure design to reduce the weight and maintain resistance [57]. However, the influence of

different bio-inspired geometry profiles on distribution of passing through mechanical load have not been studied jet. Exploring biological design could open new opportunities or generate new ideas to solve above mentioned problems.

1.3.3. Conclusions of the literature review

The following conclusion have been obtained from the literature review presented above:

- Contact performance was only analysed under physiological loading conditions in biological joints, so there is not enough information about technological advantages of these joints for their later use as a source of bioinspiration.
- The coexistence of two different morphologies for the elbow joint among different species has not been answered yet.
- No scientific evidence found relating the different joint morphologies with their load bearing performance.
- The technological limit for bearings design has been reached, as made progress is not enough to prevent their premature failure.
- Limited number of studies made with non-cylindrical geometry journal bearings.
- Use of bio-inspired geometry profile for mechanical joints design has not been studied.

1.4. Objectives

In response to the aforementioned voids in the literature, during this project evaluation of contact mechanics response of bio-inspired mechanical joints was performed. The fulfilment of the main objective is accompanied by three more specific objectives:

- Design bio-inspired mechanical joints and analyse their contact response (load bearing performance) while applying external load of two bio-inspired mechanical joints to different loading conditions.
- Determine preferential loading conditions, this is, determine under which loading conditions load bearing performance is better, where the produced peak contact pressure is lower.
- Identify how different morphologies influence on the external load bearing performance in bio-inspired mechanical joints.

With the main objective and specific objectives in mind, the design of bio-inspired mechanical joints and the analysis of their contact mechanics was carried out. The whole project is divided into three main tasks in order to achieve the main objective:

First task is related with the mechanical joints design. Their design is going to be based in bones geometries of left elbow of camel and bison collections received from the National Museum of Natural History in Paris, *Camelus bactrianus* MNHN-ZM-AE-2007-1435 and *Bison bison* MNHN-ZM-AC-1951-242.

Once the mechanical joints are designed, the second task was the analysis of the load distribution through them by means of numerical simulations of contact phenomena. Different loading conditions were applied in order to analyse their dependence, this is, the response of contact pressure distribution under different conditions.

The last task would be related to the analysis of the results and conclusions obtention. All these tasks, at the same time, are divided the into different phases. These phases can be seen in the section 'Phases of the project'.

1.4.1. Phases of the project

To achieve the objective, first, bio-inspired joints have been designed (T2). In order to achieve this task first the extraction of the profile geometry took place. In second place, once the profiles are obtained, the computer-aided design (CAD) models of the mechanical joints were created.

In second place, contact mechanics simulations (T3) were performed. Numerical contact simulation technique was used to analyse the load distribution through them by means of numerical simulations of contact phenomena. For this, meshing of the CAD models were performed in first place. On second place boundary conditions were defined and loading conditions set. In third place, via an automatized macro using Visual Basic Application (VBA), the simulations were executed.

Finally, the obtained results from the simulations were analysed (T4). For that, a statistical treatment of the results was carried out and, after that, the comparison between the different results was performed and conclusions were obtained. The develop of the project took eight months. In order to organize different phases and activities of the project Gantt diagram was made, see Table 1.2.

Table 1.2: Gantt diagram of the project.

SCHEDULE																					
Phases	Activities	November			December			January			February		March		April		May		June		
		45-46	47-48	48-49	50-51	45-50	45-51	1-2	3-4	5-6	7-8	9-10	11-12	13-14	15-16	17-18	19-20	21-22	23-24	25-26	
1. Experiment design (T1)	Literature review																				
	Initiation in finite element calculation																				
	Definition of project's objectives																				
	Definition of simulation and validation protocol																				
2. Bio-inspired joints design (T2)	Generation of the morphological profiles																				
	Creation of CAD model																				
3. Contact mechanics simulation (T3)	Meshing																				
	Boundaring conditions and loading conditions definition																				
	Simulations execution																				
4. Analysis of the results (T4)	Results treatment																				
	Comparison of the results																				
5. Report writing (T5)	Writing of the document																				
	Writing of the article																				

1.5. Conditions of the project

In this section the information of the project specification is explained. The work carried out, necessary resources, specific requirement and legal aspects to carry out the project are mentioned.

1.5.1. Work to be carried out

The objective of this work is to evaluate and compare the mechanical performances of bio-inspired joints. To achieve the objective, contact areas and maximal contact pressure are estimated and compared numerically of the different joints.

1.5.2. Resource specification

Used software's for the development of this project:

- Excel software.
- Software: NX 11.0 (Siemens, Germany) pre-post processor, Samcef 2015 V.17.1 (Samtech, Belgium) solver.
- CATIA V5

Hardware’s technical specifications

- Operating system: Windows 10 professional for workstations.
- Processor: Intel (R) Xeon (R) Gold 6134 CPU @ 3.20 GHz 3.19 GHz.
- Ram 256 Go (255 Go usable), 64 bit operating system x64 based processor.

1.5.3. Legal aspects

As far as the safety of the worker is concerned, the worker must have received the relevant information on the prevention of occupational risks. In addition, the worker must have an adequate workplace and have accident and liability insurance while on site.

1.5.4. Contractual aspects

As defined in the Learning Agreement, the project must be completed by 26th of June. By this data the report describing all the work done during the stay must be completed.

Chapter 2. Development of the project

In this chapter, detailed description of the performed tasks during the project is displayed. First, the design of the bio-inspired mechanical joints is presented. Then, the development and execution of the numerical simulations is described. The obtained results are presented. Last, the difficulties encountered during the development of the tasks and their solutions are introduced.

2.1. Detailed description of tasks

As explained before, the project was divided into three main tasks: mechanical joints design, contact mechanics simulation execution and obtained results treatment (see Figure 2.1). Each task is described in detail in the following order:

- Mechanical joints design
- Contact mechanics simulation
- Results post-processing

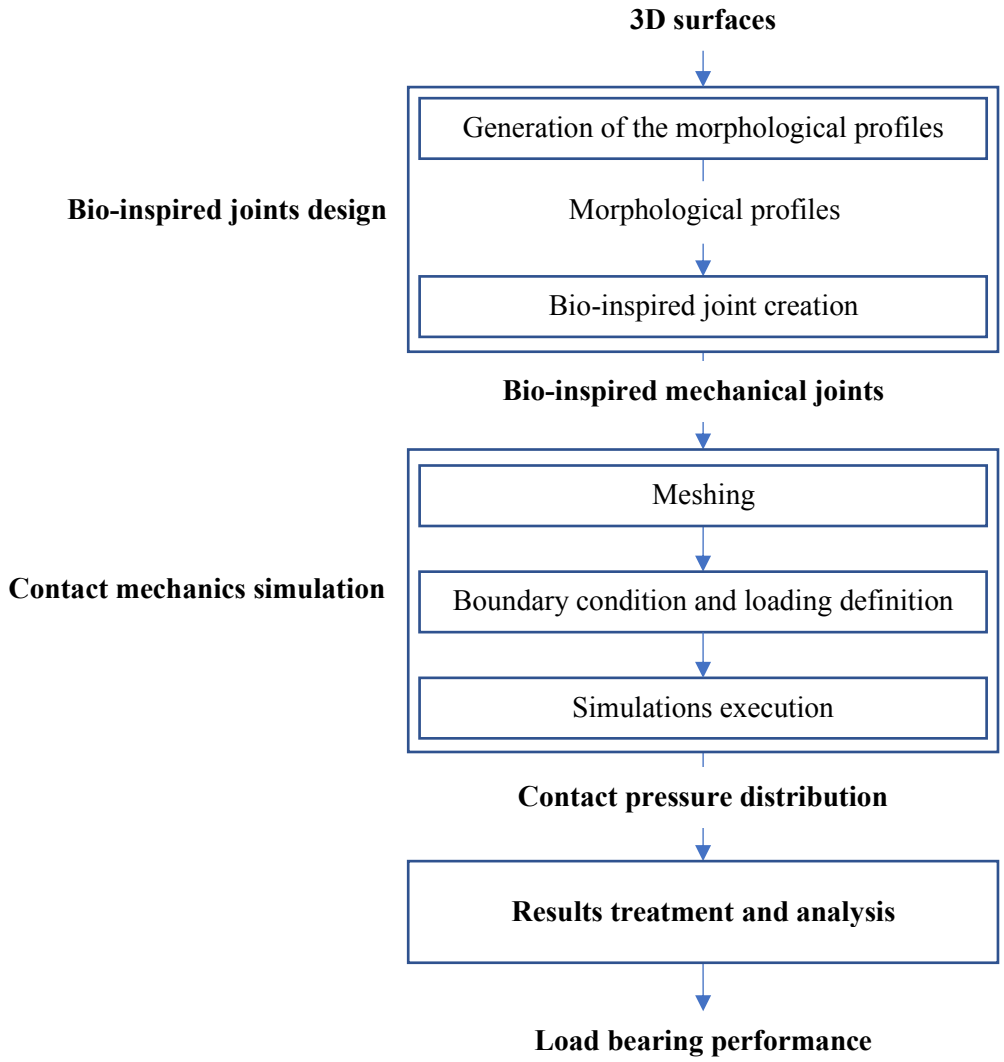

Figure 2.1: Followed methodology.

2.1.1. Bio-inspired joints design (T2)

During this first phase, the design of the mechanical joints was carried out. Two groups of mechanical joints were created: one group corresponding to the camel-inspired joints (representing the group of animals of morphology I) and the other corresponding to the bison-inspired joints (representing the group of animals of morphology II) (Figure 2.2(c)). These two animals were chosen since their elbows have similar dimensions among the animals of the two groups presented in Figure 1.2. Using bones of similar dimensions allows to modify as less as possible the original dimensions of the profiles during the creation of the mechanical joints. The idea was to modify the original geometry as less as possible to study the load bearing performance of the original elbows. Using these two animals implied a relatively small modification in the original dimensions of the joints.

Dry bone specimens (bones without soft tissue) of the left elbow from different species with the same ability of movement of the elbow joint: (a single DOF in rotation, the most similar to the industrial kinematic joints) surface scans were performed. These surfaces were scanned using a 3D optical scanner (Gom ATOS III, Braunschweig, Germany) with a resolution of 0.02 mm. The step files of the articular surfaces of camel and bison elbows were the input of this phase (Figure 2.2(a)).

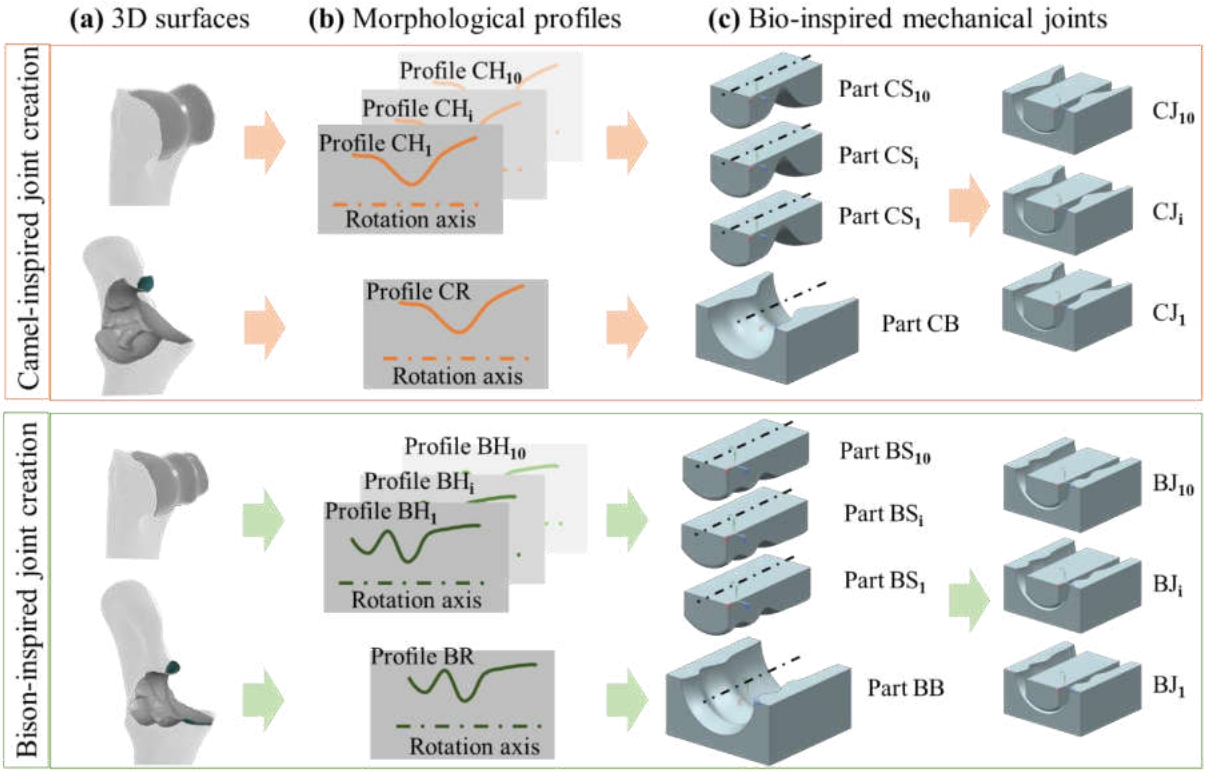

Figure 2.2: (a) Camel and bison radius-ulna and humerus 3D surfaces; (b) morphological profiles and (c) bio-inspired mechanical joints.

Contact simulations were carried out between mechanical joints. For the creation of these mechanical joints, 3D surfaces were used (Figure 2.2(a)). First, from these surfaces the morphological profiles were extracted and later the joint was created. Detailed information about these steps is explained below.

(a) Generation of the morphological profiles

For the profiles extraction 3D surfaces were used. Using CATIA V5, ten morphological profiles were obtained from each (camel and bison) humerus 3D surfaces. One radius-ulna morphological profile was obtained from each (camel and bison) radius-ulna 3D surfaces. The intention of extracting ten morphological profiles was recreating ten different flexion-extension angle position of the elbow joint. It has been demonstrated that the contact (location of the contact zones, contact area and the contact pressure) depends on the flexion-extension angle of the elbow [58]. The morphological profiles are depicted in Figure 2.3 in blue.

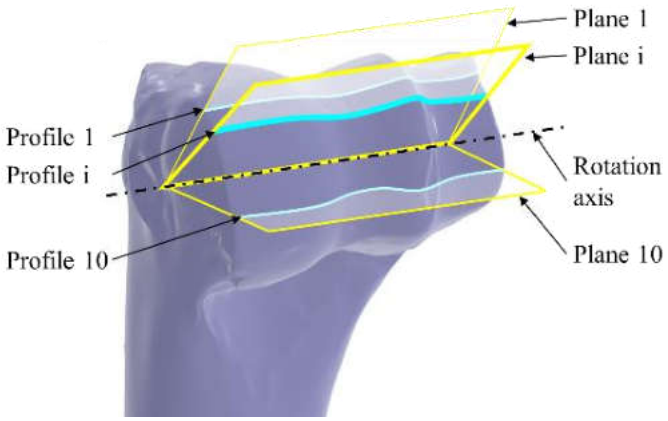

Figure 2.3: Morphological profile obtaining. In yellow colour intersection planes, in black rotation axis in blue profile examples.

The profiles were generated performing an intersection between the 3D surfaces and equiangular planes (5° of angular step) passing through the rotation axis (Figure 2.3 in yellow colour). The 3D surfaces were considered as revolution surfaces and their axes were extracted by best fitting. Camel and bison humerus morphological profiles are depicted in Figure 2.2(b).

Later the smoothing of the profiles was performed. Smoothing was performed by curvature analysis of the profiles manually, with a maximum point displacement of 0.02 mm. The smoothing operation avoided the introduction of bone degeneration details and allowed to analyse the global bearing performance of the morphology and at the same time facilitate the manufacturing if needed. Curvature analysis of camel and bison original profiles and smoothed profiles can be seen in Figure 2.4.

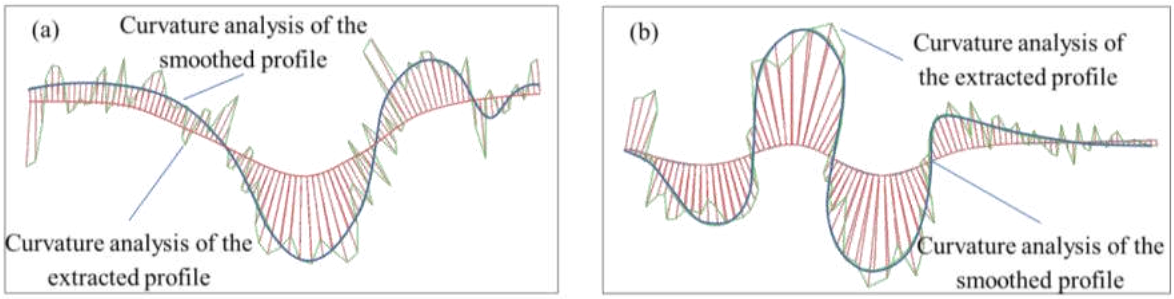

Figure 2.4: Humerus curvature analysis of the (a) camel profile and (b) bison profile.

Last, the scaling of the morphological profiles was carried on. The objective of this scaling was to obtain equivalent mechanical joints with the same average radius and length. This is necessary to make feasible the comparison of the joints in terms of load transmission. The average radius of the distal articular surface of the camel and bison humerus was of 25.3 mm and 20.1 mm respectively. Their length was of 64.3 mm and 71.7 mm respectively. A scaling was performed, and the obtained dimensions of the joints were: 68 mm of length and 22.7 mm of average radius. These morphological profiles (Figure 2.5) were used for the generation of mechanical joints.

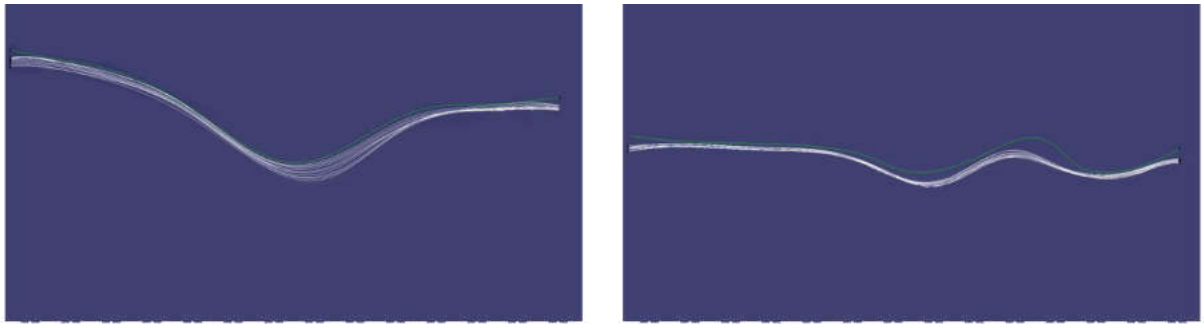

Figure 2.5: Smoothed and scaled morphological profiles (a) camel and (b) bison. White colour humerus profiles and in green colour radius-ulna profiles.

(b) Creation of the bio-inspired mechanical joints

The last step in this phase was generating the bio-inspired mechanical joints. In Figure 2.6, the bio-inspired mechanical joints can be seen in an exploded view with the overall dimensions of the parts. The bio-inspired mechanical joints were composed by two parts: shaft and bearing. For the creation of the bearing parts (for camel and bison), the radius-ulna morphological profiles were used. For the creation of the shaft parts, the humerus morphological profiles were used. Ten shaft parts were obtained for the camel and ten for the bison. Combining these shaft parts with the bearing parts, ten mechanical joints were created. Studying contact mechanics of these mechanical joints, as said before, allows to recreate the elbow at ten different flexion-extension angles. This allows also to reduce the influence of specific details of the geometry.

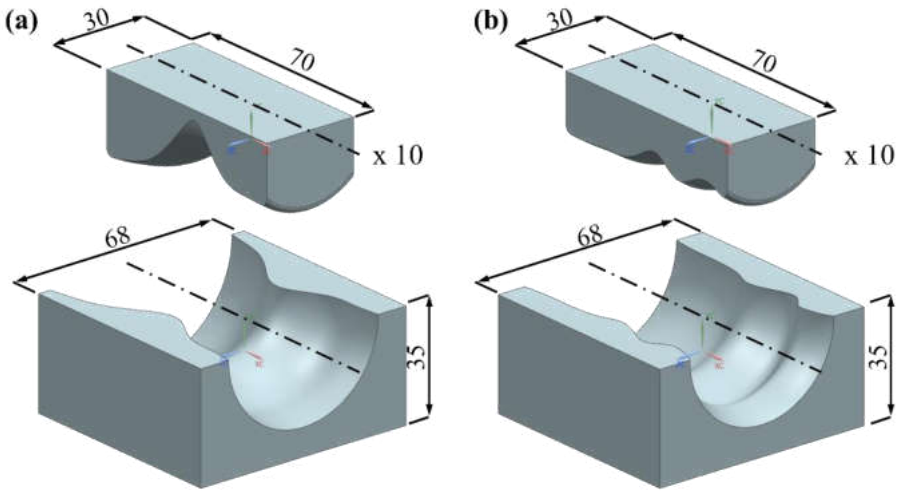

Figure 2.6: Exploded view of the mechanical joints with the overall dimensions of the parts (a) camel-inspired joint and (b) bison-inspired joint. Dimensions are expressed in mm.

The creation of the parts (shaft and bearing) was done by means of a revolution of the aforementioned profiles. The reason to use revolution surfaces is motivated by three main ideas. The first idea is to facilitate the manufacturing stage in case of needing it. The second idea is to facilitate the analysis only global behaviour of the morphology. The third idea is to avoid over pressure phenomena due to irregularities of the surface along the radial direction. The shaft parts were considered of 4340 alloy steel (Young's modulus of 193000 MPa and Poisson's ratio of 0.28). The bearing parts were considered of polyoxymethylene (Young's modulus of 3000 MPa and Poisson's ratio of 0.35). Both materials were linear elastic and isotropic. The mass of the shaft part of the camel-inspired joint was of 325.8 g while of the bison-inspired joint was 306.9 g.

Bio-inspired mechanical joints models have been exported to the NX 11.0 software (Siemens, Germany) [59] by means of .stp files in order to perform numerical simulations of contact phenomena using finite element method (FEM).

2.1.2. Contact mechanics simulations (T3)

Once the geometries were created, contact simulations were performed by the FEM using commercial finite element package NX solver and Samcef 2015 V.17.1 pre-post processor. The analysis was done assuming small displacements and deformation, using isotropic materials.

Along this section, the numerical FEM models for the contact analysis of the camel-inspired and bison-inspired mechanical joints are presented. This section is divided into three

subsections. First, the meshing of the CAD models is presented in Section (a). Second, the definition of the boundary conditions and the external loads (axial load, radial load and turnover moment) is described in Section (b). Third, the execution of the simulations is explained in Section (c).

(a) Meshing

First step of contact mechanics simulation was the meshing definition. While analysing the contact by FEM is important to choose the meshing elements size and type that best fits with the model. The quality and density of the mesh directly impact on the results of finite element analysis as well as the calculation time [60]. In order to verify the information about different meshing elements types and accuracy, a simplified model of contact between two cylinders was created. Using this simple model, the contact response was analysed with respect to different meshing elements. It was concluded that hexahedral elements of eight nodes have better performance for contact mechanics problems. Detailed information about the performed numerical contact simulations with simplified model can be seen in Section Meshing convergence analysis.

Shaft and bearing parts were imported into NX 11.0 software and meshed individually using hexahedral linear elements. It has been demonstrated that this type of elements behave better for contact mechanics problems [61].

Another mesh convergence analysis was performed to determine the appropriate mesh size with elements with average edge lengths of approximately of 0.5 mm, 1 mm and 2 mm. Elements with average edge lengths of approximately 1 mm were found to provide an acceptable compromise between result accuracy and computational efficiency. The average number of elements, nodes and degrees of freedom per model are indicated in Table 2.1. In Figure 2.7, the meshed models of (a) camel-inspired joints and (b) bison-inspired joint are shown.

Table 2.1: Average number of elements, nodes and DOF of the numerical models of the mechanical joints.

Model	N° of elements	N° of nodes	DOF
Camel	39600	53502	1891
Bison	41400	55393	1891

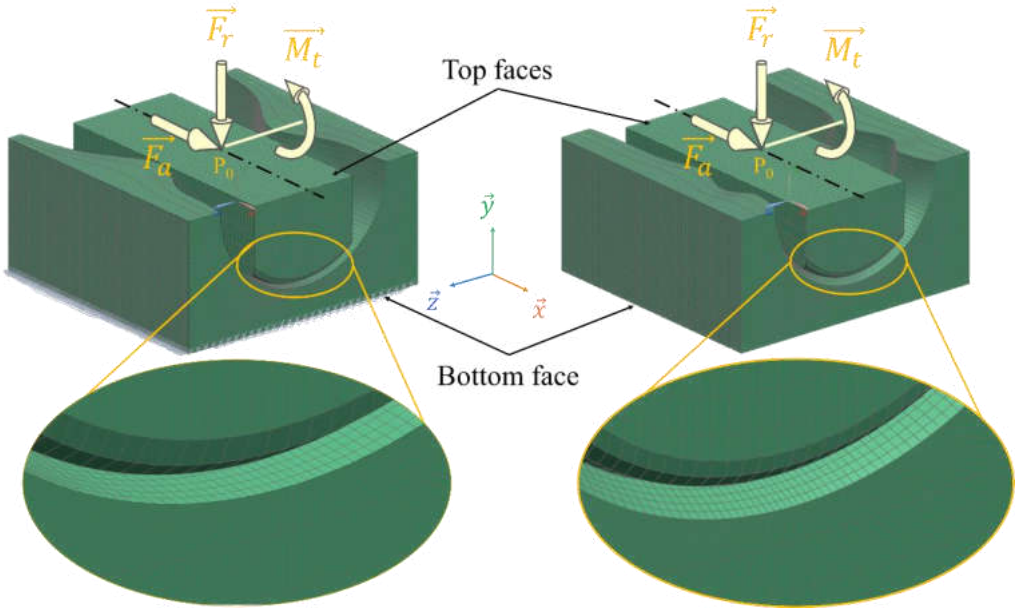

Figure 2.7: Example of used meshing size in (a) camel-inspired joint; (b) bison-inspired joint. A detail can be seen of the meshing's on the lower part of the model. P_0 point indicates the joint centre point. $\overrightarrow{F_a}$ represents the direction of the axial force. $\overrightarrow{F_r}$ represents the radial force. $\overrightarrow{M_t}$ represents the turnover moment. Represented loads are assumed positive in the axis direction.

1. Meshing convergence analysis

For the verification of different meshing elements accuracy, a simplified model of two cylinders was created. Contact mechanics problem was performed using this simple model and the contact response was analysed with respect to different meshing elements. In Figure 2.8 can be seen the CAD model of the simplified model of two cylinders.

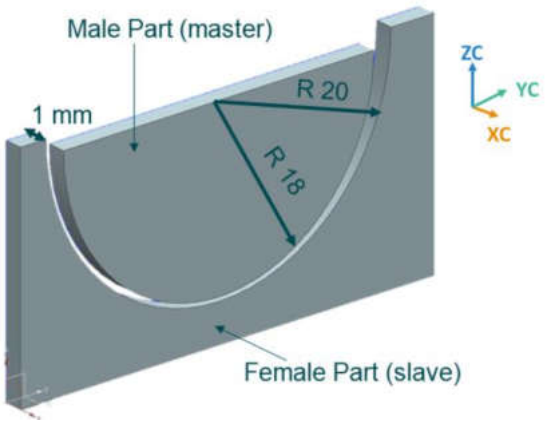

Figure 2.8: CAD model of simplified two cylinders for contact simulation.

To calculate the theoretical value of maximum contact pressure Hertzian equations for cylindrical contact have been used, (1) and (2).

$$b = \sqrt{\frac{2F}{\pi l}\frac{\frac{1-{v_1}^2}{E_1}+\frac{1-{v_2}^2}{E_2}}{\frac{1}{d_1}+\frac{1}{d_2}}} \quad (1)$$

$$P_{max} = \frac{2F}{\pi b l} \quad (2)$$

Where:

b: contact half-width

P_{max}: maximum pressure

F: Applied force

l: Contact length of cylinders

v_1: Object-1 Poisson's ratio

v_2: Object-2 Poisson's ratio

E_1: Object-1 elastic modulus

E_2: Object-2 elastic modulus

d_1: Object-1 diameter

d_2: Object-2 diameter

Four different meshing elements have been analysed (as shown in Figure 2.9): Hexa linear (8 nodes), Hexa quadratic (20 nodes), Tetra linear (4 nodes) and Tetra quadratic (10 nodes). For all of them elements with edge lengths of approximately 0.2 mm were set.

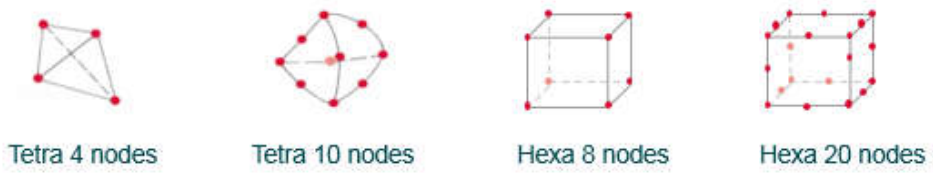

Figure 2.9: Analysed meshing elements.

Used material for both cylinders: Titanium Ti-6Al-4V, on its linear elastic behaviour, no plastic deformation, isotropic, $v_1 = v_2 = 0.34$ and $E_1 = E_2 = 121\,000\ {}^{\mathrm{N}}/_{\mathrm{mm}^2}$.

The defined boundary conditions were the following ones: female part fixed to the ground, male part free movement in Z and Y axes and $F = 100$ N applied on the upper side of male part, Figure 2.8.

Between simulation properties uncoupled, frictionless and unidirectional contact between surfaces were defined. The simulation was performed by a Linear Static analysis using Samcef solver in NX software. Obtained results can be seen in Table 2.2 and surface contact pressure distribution in Figure 2.10.

Table 2.2: Cylinders contact simulation results.

Mesh	Time	P_{max} (MPa)	Relative error to theorical value (%)	Strain energy error (%)
Theoretical value	-	155.55	-	-
Hexa (8)	38 s	156.882	0.85	-
Hexa (20)	2 min 40 s	223.32	30.34	-
Tetra (4)	53 s	166.98	6.85	23.80
Tetra (10)	3 min	165.63	6.08	3.43

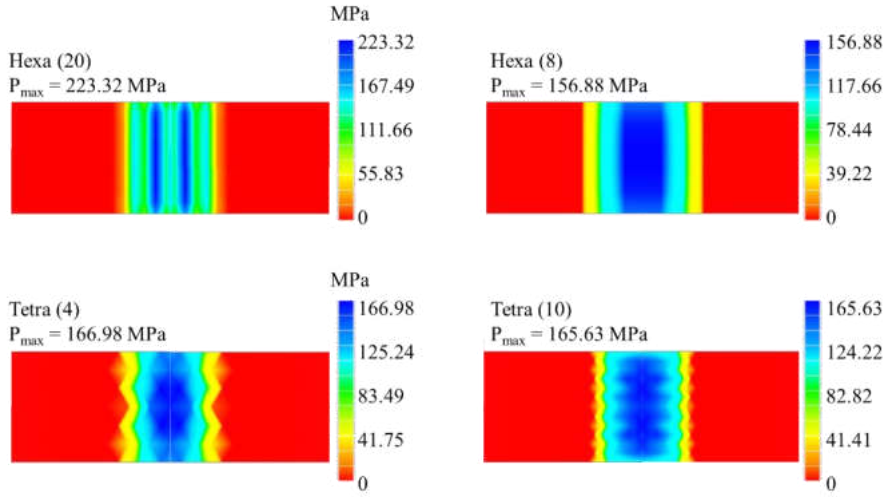

Figure 2.10: Surface contact pressure distribution along the female part a simplified model of two cylinders.

From the obtained results in Table 2.2 and Figure 2.10, it was concluded that hexahedral elements of eight nodes have better performance for contact mechanics problems as in the performed analysis, experimental result with this elements had the closest response to the theoretical value.

(b) Boundary conditions and loading definition

The shaft and bearing parts were initially assembled making coincident their rotation axes and their lateral faces parallel and aligned (as seen in Figure 2.7). All the degrees of freedom were restricted in the bottom face of the bearing parts. Rotation around $\vec{x}$ and $\vec{y}$ axes was restricted on the top face of the shaft parts. The inner surfaces of the bearing parts were selected as slaves, and the outer surfaces of the shaft parts were selected as masters. Unidirectional and frictionless surface-to-surface contact was defined between slave surface and master surface. The contact was analysed on the master surfaces.

Three simulations sets were defined to evaluate the bearing performance regarding axial load, turnover moments and combined loads of the created joints. For a feasible comparison, the magnitude between the of the applied load was the same and equal to 5.2 kN for all simulations. It was assumed that all loads act in the same plane in all simulation sets.

Table 2.3: Loading conditions for the set of numerical simulations to study bearing performance regarding axial loads. Horizontally, the axial load and radial load values are indicated. On the left column is indicated the turnover moment.

F_r (kN)	4.886	5.023	5.121	5.180	5.200	5.180	5.121	5.023	4.886	4.713	4.503
F_a (kN)	-1.779	-1.346	-0.903	-0.453	0.000	0.453	0.903	1.346	1.779	2.198	2.600
M_t (Nm)											
F_r*(-26.5)	Sc1	Sc13	Sc25	Sc37	Sm1	Sc49	Sc61	Sc73	Sc85	Sc97	Sc109
F_r*(-22.1)	Sc2	Sc14	Sc26	Sc38	Sm2	Sc50	Sc62	Sc74	Sc86	Sc98	Sc110
F_r*(-17.7)	Sc3	Sc15	Sc27	Sc39	Sm3	Sc51	Sc63	Sc75	Sc87	Sc99	Sc111
F_r*(-13.3)	Sc4	Sc16	Sc28	Sc40	Sm4	Sc52	Sc64	Sc76	Sc88	Sc100	Sc112
F_r*(-8.8)	Sc5	Sc17	Sc29	Sc41	Sm5	Sc53	Sc65	Sc77	Sc89	Sc101	Sc113
F_r*(-4.4)	Sc6	Sc18	Sc30	Sc42	Sm6	Sc54	Sc66	Sc78	Sc90	Sc102	Sc114
F_r*(0)	Sa1	Sa2	Sa3	Sa4	Sa5	Sa6	Sa7	Sa8	Sa9	Sa10	Sa11
F_r*(4.4)	Sc7	Sc19	Sc31	Sc43	Sm7	Sc55	Sc67	Sc79	Sc91	Sc103	Sc115
F_r*(8.8)	Sc8	Sc20	Sc32	Sc44	Sm8	Sc56	Sc68	Sc80	Sc92	Sc104	Sc116
F_r*(13.3)	Sc9	Sc21	Sc33	Sc45	Sm9	Sc57	Sc69	Sc81	Sc93	Sc105	Sc117
F_r*(17.7)	Sc10	Sc22	Sc34	Sc46	Sm10	Sc58	Sc70	Sc82	Sc94	Sc106	Sc118
F_r*(22.1)	Sc11	Sc23	Sc35	Sc47	Sm11	Sc59	Sc71	Sc83	Sc95	Sc107	Sc119
F_r*(26.5)	Sc12	Sc24	Sc36	Sc48	Sm12	Sc60	Sc72	Sc84	Sc96	Sc108	Sc120

In the simulation set 1 (the conditions of the simulation set 1 can be seen in Table 2.3 in blue colour denominated as Sa*i*), bearing performance regarding axial loads (F_a) was analysed. The studied range of axial load went from -2.6 kN to 2.6 kN. The turnover moment was zero for these simulations. The applied radial load was calculated in function of the applied axial load in order to obtain a load equal to 5.2 kN. Simulation set 1 was performed with all the joints of both groups (camel and bison-inspired joints).

In the simulation set 2 (the conditions of this simulation set can be seen in Table 2.3 in brown colour denominated as Sm*i*), the bearing performance regarding turnover moments (M_t) was analysed. The axial load was zero for these simulations. The studied range of turnover moment went from -138 Nm to 138 Nm. An off-centred load of 5.2 kN was applied in radial direction to obtain the desired moment value. Simulation set 2 was performed with all the joints of both groups (camel and bison-inspired joints).

The simulation set 3 aimed to analyse the bearing performance regarding combined loads (axial loads and turnover moments). The analysed loading conditions in the simulation set 3 can be seen in black colour, and they are denominated as Sc*i*. This simulation set was performed only with one geometry of each group (one for camel and one for bison) due to computational costs. This geometry was chosen as that whose response was the closest to the average response of all the geometries analysed. The analysed range of axial load went from -2.6 kN to 2.6 kN and the analysed range of turnover moment went from -138 Nm to 138 Nm.

(c) Simulations execution

A total of 720 numerical simulations of contact were performed for both group of joints (camel-inspired and bison-inspired joints). All the simulations were performed using Samcef 2015 V.17.1 (Samtech, Belgium) solver on a desktop computer (Intel (R) Xeon (R) Gold 6134, 256 Go RAM, running a 64-bit operating system). The initial contact stiffness was set on 2000 N/mm^3 and the maximum allowable penetration depth 0 mm. The problem was solved using linear static analysis (assuming small displacements and deformation) and uncoupled iteration method. Each simulation took approximatively one minute. To launch the simulations Macro VBA automatization code was used. This code can be seen in Appendix A.

2.1.3. Results treatment (T4)

Using NX as postprocessor, the highest contact pressure values were averaged and considered as the peak contact pressures (P_{max}). This with the aim of mitigating numerical errors due to the discretisation of the geometry during the meshing process.

For the simulations set 1 (variation of axial force) and 2 (variation of turnover moment), the mean of the results ($\overline{P_{max}}$) of the different geometries and the coverage interval were calculated. Coverage intervals were determined as twice the standard deviation. From these results, the geometry whose response was the closest to the average response of all the geometries was chosen for the simulations set 3.

2.2. Presented problems and proposed solutions

2.2.1. Poor concordance between the real bones and designed mechanical joints

It was seen that the geometry of the articular surface slightly variates along the radial direction of the elbow joints of the two animals. Due to the difficulties that the reproduction of this geometry would introduce in manufacturing stage, it was decided to model the joints as revolute joints. During the first two months of the project the simulations were performed on camel-inspired and bison-inspired joints designed based on the average profile of the scanned surfaces. Finally, they were discarded because they were not representative of the real bone geometry along the radial direction. In order to take into account the variability of the morphology of the articular surfaces along the radial direction, ten revolute joints were designed. These revolute joints recreated ten morphologic profiles representing ten different flexion-extension angle positions of the elbow.

2.2.2. Edge effect appearing

During the first simulations carried out, it was observed that a high concentration of the pressure in a reduced area occurred (edge effect phenomenon), very abrupt contact results in the corners of the geometry (Figure 2.11). To neutralize this effect, a two-millimeter rounding of the edges to the male parts was performed (Figure 2.12).

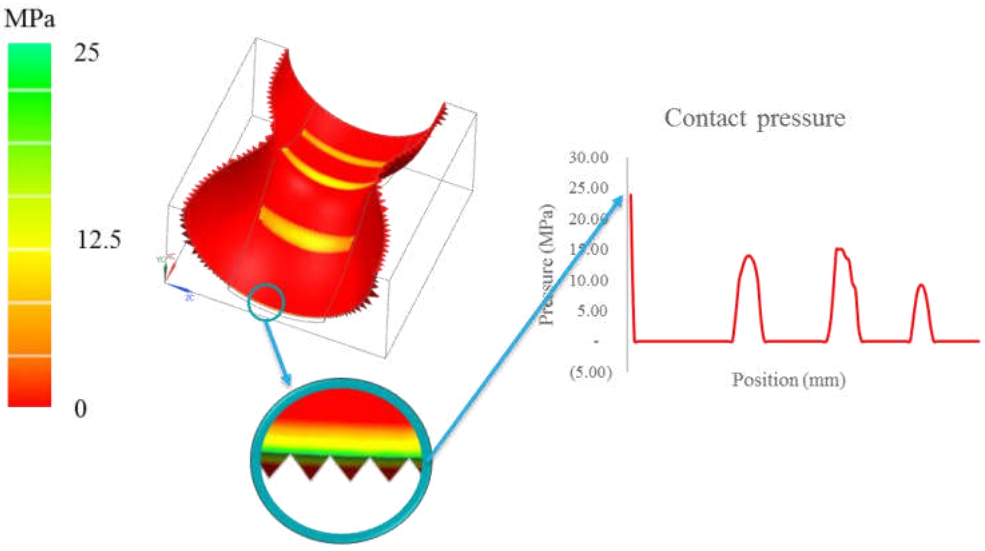

Figure 2.11: Example of edge effect (green colour) without rounding with camel-inspired joint.

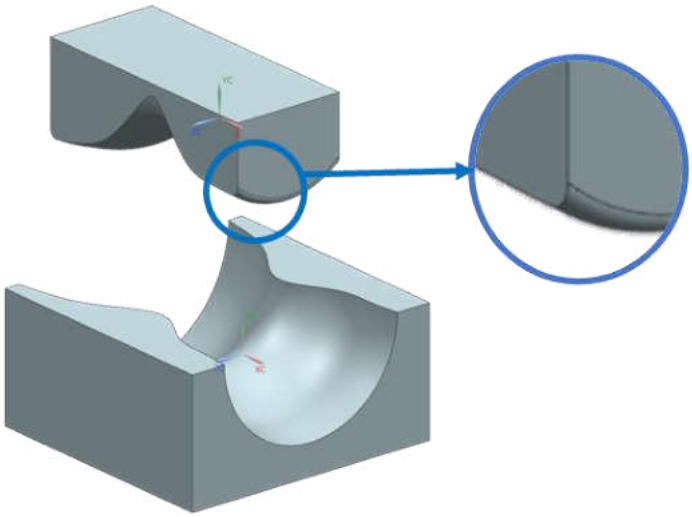

Figure 2.12: Example of rounding of the edge in camel-inspired joint.

2.2.3. Uncertainty created during simulations

To analyse the contact pressure distribution, contact pressure was considered in each simulation. Simulation may introduce numeric approximations. To reduce the effect of the numeric approximations in each simulation five highest values of peak contact pressure were determined, and their average was considered as peak contact pressure (P_{max}). In order to minimize numeric errors, results for the same loading conditions were analysed together and not individually, calculating average peak contact pressure value ($\overline{P_{max}}$).

2.2.4. Boundary condition and loading definition

For loading conditions definition several times individual simulations were run. In them the limit of axial and turnover moment conditions that the geometries can support were determined. In addition, initially the idea of this project is thought for its later experimental analysis. So, the boundary conditions were defined based on the conditions that must be followed with an experimental model to verify the results for their greater similarity.

2.2.5. Simulation conditions and meshing definition

To determine the proper simulation conditions a simplified model was used. With this model, contact problem was solved theoretically using Hertzian equations and numerical simulations were performed under different simulation conditions. The simulation conditions were seen to have little influence on the results. The parameters that had the closest result to the theoretical value were chosen for the mechanical joints simulations.

Regarding to the meshing, the same simplified model was used for meshing convergence analysis using different meshing types. Simulations were launched and it was seen that hexahedral elements had the closest response. Detailed explanation in Section Meshing convergence analysis**.**

2.2.6. Not enough pronounced trend due to low load

The first simulations were carried out with a total load of 1300 N. It was expected to see a clear dependence between the peak contact pressure result and loading conditions. Since the load was very low, a similar behaviour was obtained in both joints and very linear response. It was decided to repeat the simulations by increasing the load to 5200 N in order to see the effect augmented.

2.2.7. Waste of time in manual simulations launching

A simulation set of fifty different loading conditions had to be launched with twenty mechanical joints. Launching manually a set of so many simulations with so many geometries takes a lot of time. It was decided to invest time to automate the process designing a macro VBA to launch the simulations by itself. This macro had to be launched once for each geometry and automatically solved the simulations, saving time. The macro VBA codes used for simulations launching can be seen in Appendix A.

Chapter 3. Results of the project

In this chapter are displayed, detailed and analysed the results obtained from the numerical simulations. For each simulation contact pressure between articular surfaces was analysed and peak contact pressure was determined. The results are presented, first, regarding axial load, in second place regarding turnover moment and last regarding combined loads. Also, regarding the results, some of the obtained conclusions of the research are exposed.

3.1. Results of the numerical simulations

A total of 720 numerical simulations of contact were performed for both group of joints (camel-inspired and bison-inspired joints) under different conditions seen in Table 2.3. Only converged finite element solutions are reported and discussed. Peak contact pressure values are reported in function of the applied external loads (axial load, turnover moment and combined loads) in the following sections. One of the purposes of these simulations is to obtain the loading conditions where the load passes through the joints generating lower peak contact pressure. These loading conditions are considered as the preferential loading conditions of the joints.

3.1.1. Bearing performance regarding axial load

The applied turnover moment was zero for these simulations and axial and radial load value was variated. In Figure 3.1, P_{max} as a function of the applied axial load is presented for camel-inspired joints, on the left-hand side, and bison-inspired joints, on the right hand-side. A secondary axis represents the applied radial load. For each axial load value, points represent P_{max} values of each joint.

From the performed contact simulations, slightly different results were obtained for each joint. Each joint works somehow differently under different conditions. This could indicate that: as joints represent different flexion-extension angles, the preferential loading conditions for the best load transmission may vary according the flexion-extension angle. This could indicate that load is differently transmitted and the contact zones vary under different flexion-extension angle, showing an accordance with this article [58]. As the aim is to analyse the global trend of the morphology, the average values ($\overline{P_{max}}$) were calculated from these results and are analysed below (Figure 3.2). The goal is to obtain under which conditions the load passes through the joints generating lower peak contact pressure, considered as the preferential loading conditions. The contact areas of the closest joints to the average response of each group were analysed (Figure 3.3).

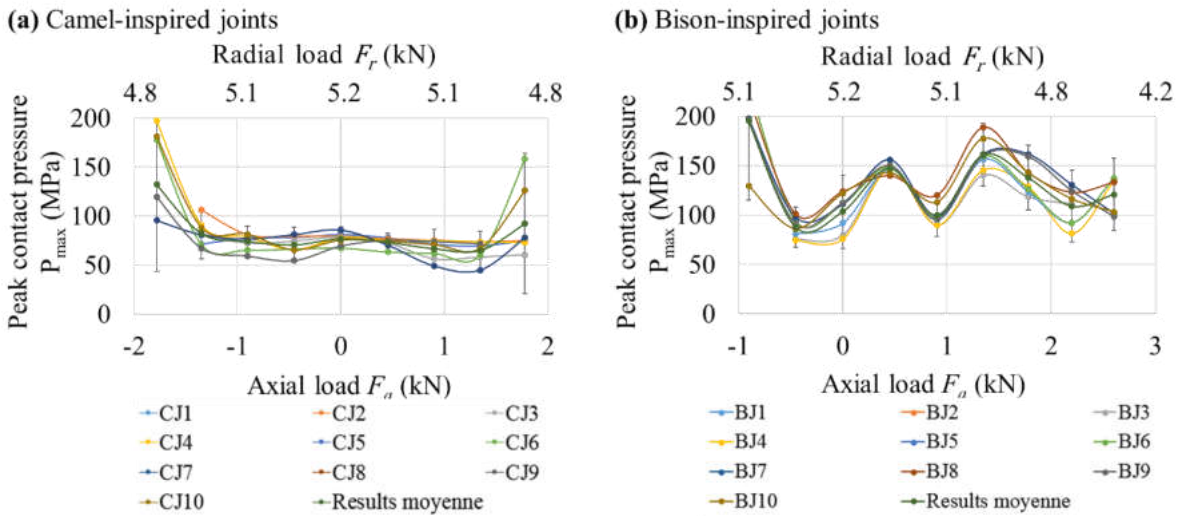

Figure 3.1: Peak contact pressure values in function of axial load are presented for the ten (a) camel-inspired joints and (b) bison-inspired joints.

In Figure 3.2, $\overline{P_{max}}$ as a function of the applied axial load is presented. A secondary axis represents the applied radial load. The applied turnover moment was zero for these simulations. For each axial load value, central points (orange triangles for camel and green circles for the bison) represent $\overline{P_{max}}$ value. The coverage interval for each set of results is represented also in Figure 3.2 (orange shading for camel and green shading for bison).

In Figure 3.2, an asymmetrical response of the $\overline{P_{max}}$ value with respect to the zero axial load value can be observed for the bison-inspired joints. It can be noticed that the camel-inspired joint was able to transmit axial loads from -1.77 kN to 2.19 kN and bison-inspired joint from -0.9 kN to 2.6 kN. An asymmetrical response of the $\overline{P_{max}}$ value with respect to zero axial load value can be seen for both joints. Analysing the convergence range of these joints, the capacity to support positive axial loads was 45% greater regarding to the capacity to support negative axial loads. Camel-inspired joints had a constant and more symmetrical response, even if the capacity to support positive axial loads was slightly greater (19%) regarding to the capacity to support negative axial loads. Bison-inspired joints had a greater capacity to support positive axial loads (65%) regarding to the capacity to support negative axial loads. Comparing the response of both set of joints, it can be noticed that camel-inspired joints had a greater capacity (49% higher than bison) to support negative axial loads. Regarding to the supported positive axial loads, bison-inspired joints had a greater capacity (18%) in comparison with camel-inspired joints.

Camel-inspired joint had lower peak contact pressures almost in all range except from 2.19 kN to 2.60 kN. The $\overline{P_{max}}$ value for all simulations of the set 1 was on average 37% lower

for the camel-inspired joint than for the bison-inspired joint. The minimum $\overline{P_{max}}$ value for the bison-inspired joints was 87.78 MPa, which was obtained under an axial load of -0.45 kN. The minimum $\overline{P_{max}}$ value for the camel-inspired joint was 36% lower than that of the bison, and it was obtained under axial load of 1.34 kN.

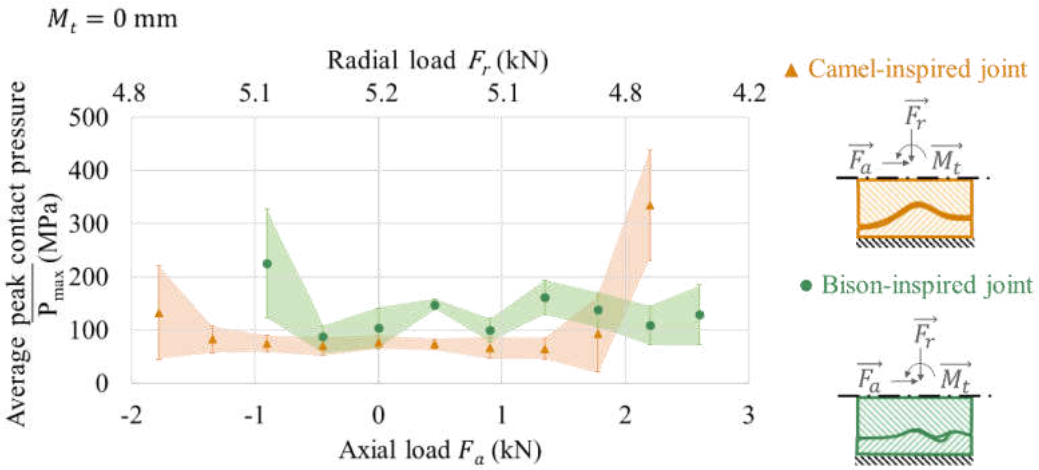

Figure 3.2: Average peak contact pressure values in function of axial load are presented for the ten camel-inspired (orange) and bison-inspired joints (green).

Among the ten tested joints (for bison and camel), those whose response was the closest to the average response of all the geometries were: joint N°2 (CJ_2) in the case of camel-inspired joints group and joint N°6 (BJ_6) in the bison-inspired joints group. These two joints were used for the following analysis of the contact areas (Figure 3.3).

Figure 3.3 shows the contact distribution, from a bottom view, on the shaft part of CJ_2 and BJ_6 for different values of axial loads. The bearing part is represented in wireframe. In this figure, it can be noticed that the contact occurs mainly near the shaft ends in both BJ_6 and CJ_2. For the considered loading conditions, the deepest part of the capitellotrochlear sulcus did not enter in contact in CJ_2 neither in BJ_6, the reason is discussed in Figure 3.10. Application of negative axial loads on BJ_6 generates a high concentration of the pressure in a reduced area (edge effects). At axial load of 1.77 kN, BJ_6 did not converge while CJ_2 did. The static equilibrium could not be satisfied under the applied conditions in this case. For the same conditions, in most of the cases, the CJ_2 had lower P_{max} values and larger contact areas than the BJ_6.

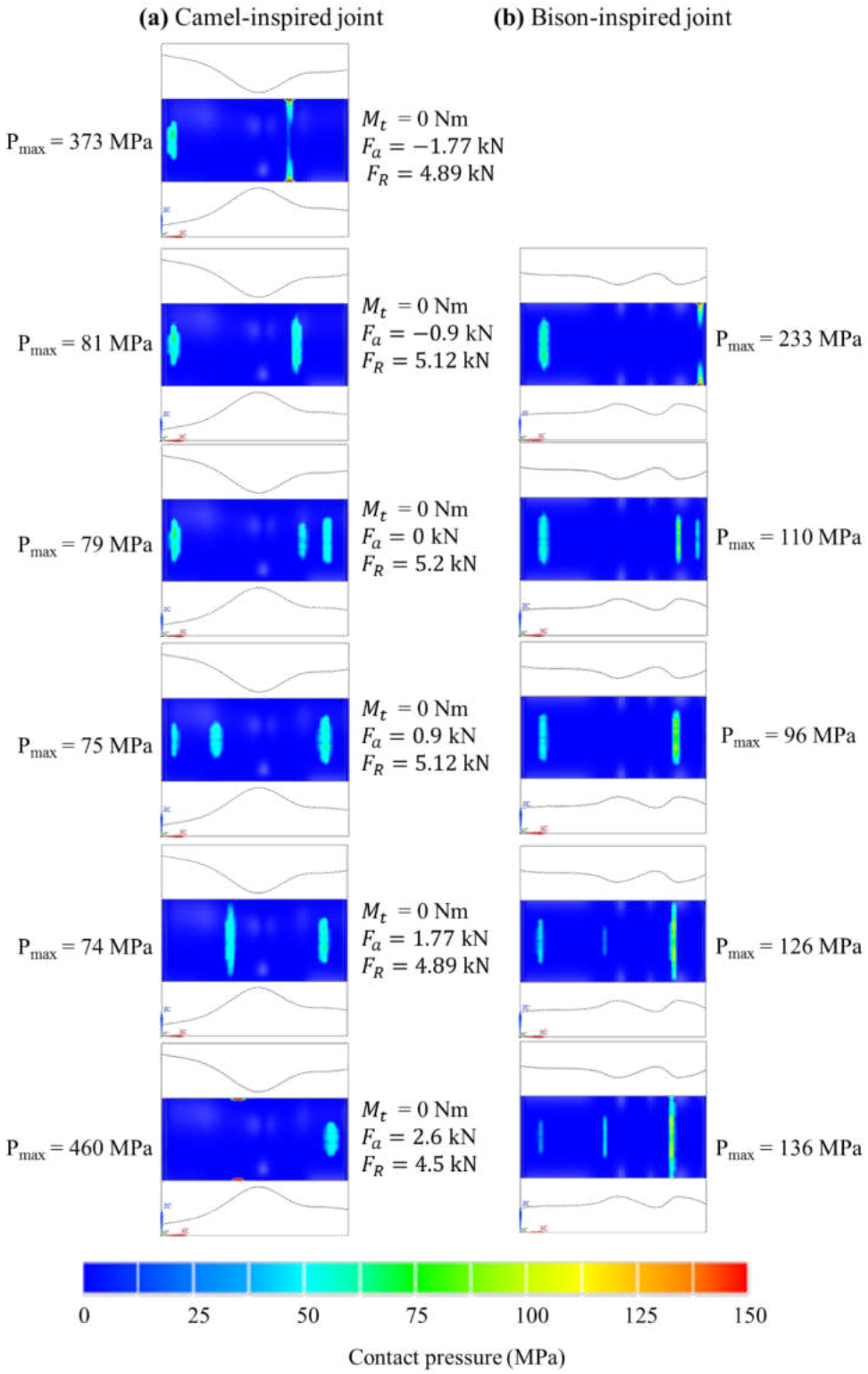

Figure 3.3: Pressure distribution on the shaft part under application of axial load (a) CJ_2 and (b) BJ_6. The applied load conditions (turnover moment, axial load and radial load) can be seen on the central part and were the same for camel and bison joints.

3.1.2. Bearing performance regarding turnover moments

The applied axial load and the radial load were constant for these simulations, 0 kN and 5.2 kN respectively, and the applied turnover moment was variated. In Figure 3.4, P_{max} as a function of the applied turnover moment is presented for camel-inspired joints, on the left-hand side, and bison-inspired joints, on the right hand-side. For each turnover moment value, points represent P_{max} values of each joint.

From the performed contact simulations, similar as in Figure 3.1, slightly different results were obtained for each joint. Each joint works somehow differently under different conditions showing an accordance with this article [58]. As the aim is to analyse the global trend of the morphology, the average values ($\overline{P_{max}}$) were calculated from these results and are analysed below (Figure 3.5). The contact areas of the closest joints to the average response of each group were analysed (Figure 3.6).

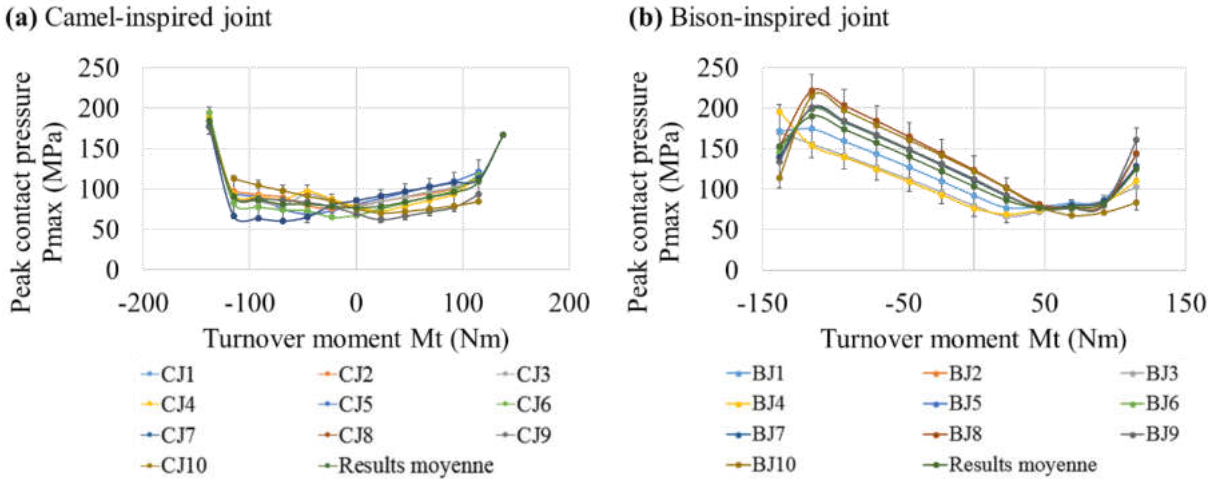

Figure 3.4: Peak contact pressure values in function of turnover moments are presented for the ten (a) camel-inspired joints and (b) bison-inspired joints.

In Figure 3.5, $\overline{P_{max}}$ as a function of the applied turnover moments is presented. The applied axial load was zero and the radial load was 5.2 kN for these simulations. For each turnover moment value, central points (orange triangles for camel and green circles for the bison) represent $\overline{P_{max}}$ value. The coverage interval for each set of results is represented also in Figure 3.5 (orange shading for camel and green shading for bison).

In Figure 3.5, an asymmetrical response of the $\overline{P_{max}}$ value with respect to the zero turnover moment value can be seen especially in bison-inspired joints. On the contrary, camel-inspired joint had more constant response. When positive turnover moments were applied, bison-inspired joints produced lower $\overline{P_{max}}$ (better load distribution) than when negative

turnover moments were applied. For the coverage interval of the bison-inspired joint of negative turnover moments was larger than for positive turnover moments.

Camel-inspired joint had lower $\overline{P_{max}}$ almost in all range except from 46 Nm to 92 Nm. Camel-inspired joint $\overline{P_{max}}$ was 86 MPa while bison-inspired joint 122 MPa. The $\overline{P_{max}}$ value for all simulations of the set 2 was on average 30% lower for the camel-inspired joint than for the bison-inspired joint. The minimum $\overline{P_{max}}$ value for camel-inspired joint was obtained under turnover moment of 0 Nm. The minimum $\overline{P_{max}}$ value for bison-inspired joint was obtained under turnover moment of 46 Nm. Both values were almost the same around 76.85 MPa.

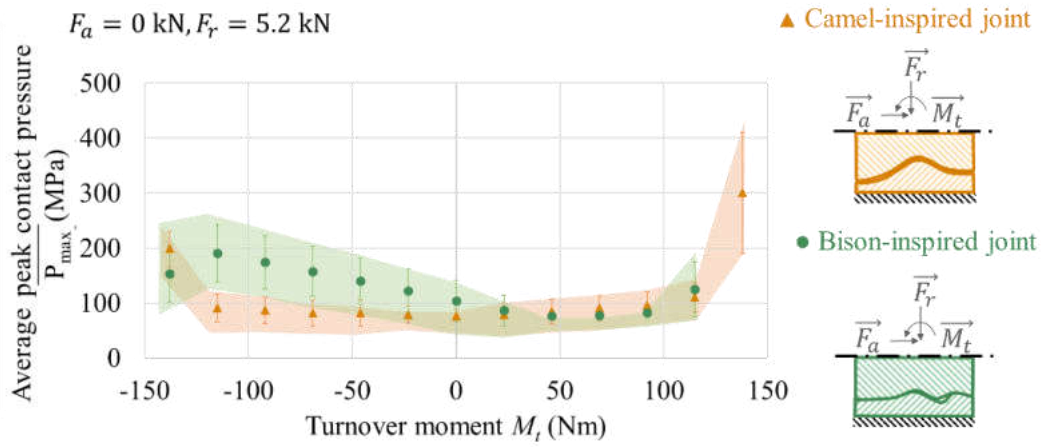

Figure 3.5: Average peak contact pressure values in function of turnover moment are presented for the ten camel-inspired (orange) and bison-inspired joints (green).

As seen in Section Bearing performance regarding axial load, among the ten tested joints (for bison and camel) CJ_2 and BJ_6 were the closest to the average response of all the geometries. These two joints were used for the following analysis of the contact areas Figure 3.6

Figure 3.6 shows the contact distribution, from a bottom view, on the shaft part of CJ_2 and BJ_6 for different values of turnover moments. The bearing part is represented in wireframe. In this figure, it can be noticed that the contact occurs mainly near the shaft part ends in both cases. Also, it was seen that under the explored range of conditions the deepest part of the capitellotrochlear sulcus never came in contact in CJ_2 neither in BJ_6, the reason is discussed in Figure 3.10. At 130 Nm bison did not converge while CJ_2 did. The static equilibrium could not be satisfied under the applied conditions in this case. For the same conditions, in most of the cases, the CJ_2 had lower P_{max} values and larger contact areas than the BJ_6.

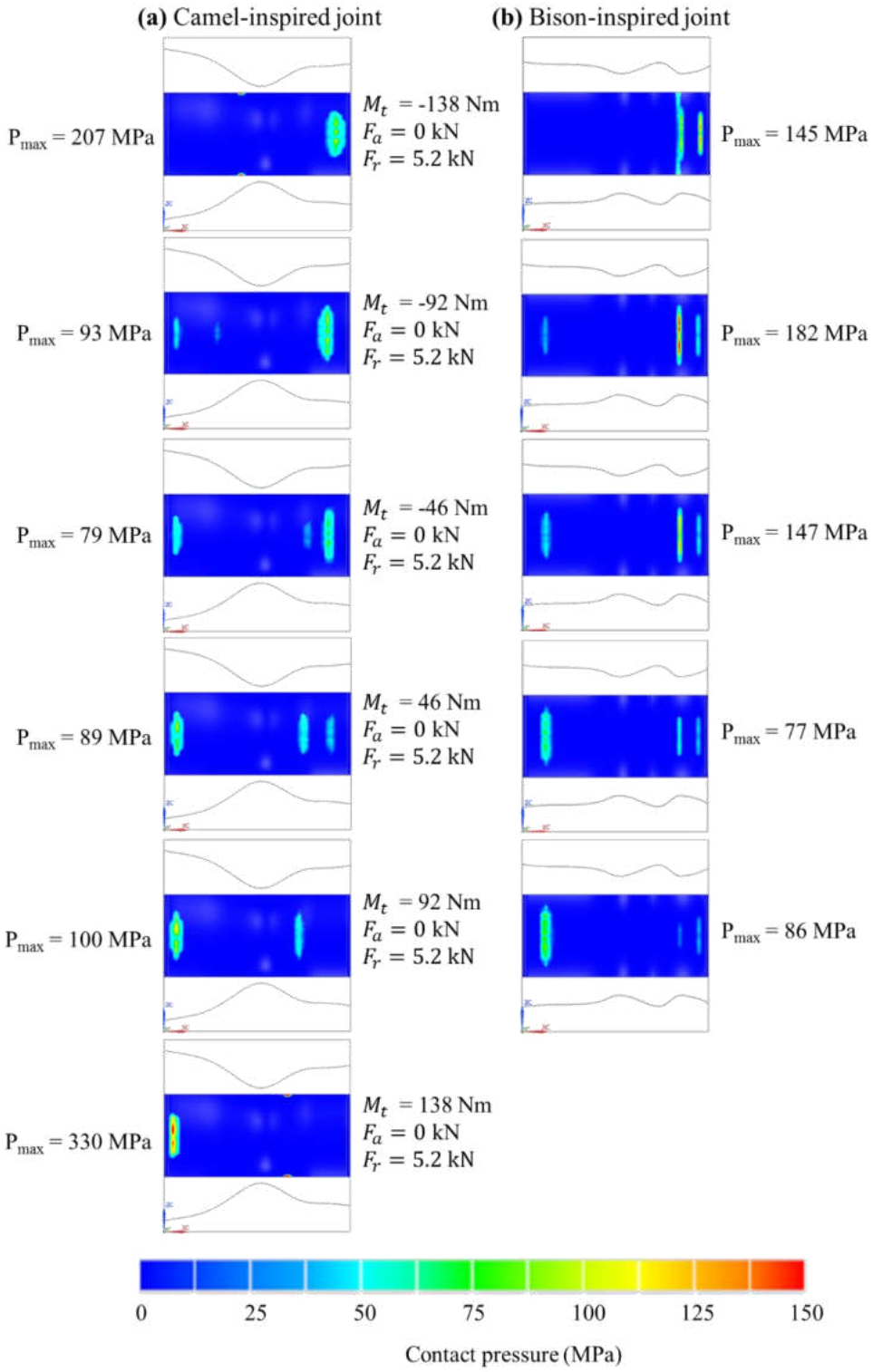

Figure 3.6: Pressure distribution on the shaft part under application of turnover moment (a) CJ_2 and (b) BJ_6. The applied load conditions (turnover moment, axial load and radial load) can be seen on the central part and were the same for camel and bison joints.

3.1.3. Bearing performance regarding combined load

On the Figure 3.7 can be seen the P_{max} response as function of the applied axial load and turnover moment of (a) CJ_2 and (b) BJ_6. On the right side the colour bar can be seen. The colour bar shows the P_{max} values from 50 MPa (in blue colour) to ≥ 130 MPa (in dark red colour). The axial load axis is represented on the horizontal axis on the left side of the graph. The range of the axial load goes from -3 kN to 3 kN. Parallel to this axe is represented the radial load axis. In the middle of the graph, in the horizontal axis, is represented the turnover moment. Turnover moment range goes from -138 Nm to 138 Nm.

In Figure 3.7 (a), as said before, it can be seen the P_{max} response of CJ_2 as function of the applied axial load and turnover moment. Regarding lowest peak contact pressures (< 90 MPa) in this figure can be seen that, in the range of the analysed loading conditions, CJ_2 behaves well under axial loads. Following this condition, CJ_2 joint had very stable behaviour on axial negative and positive loads. CJ_2 behaves well under positive and negative turnover moments. CJ_2 was able to support combined loads under the following conditions: positive turnover moments and positive axial loads; and negative turnover moments and negative axial loads. CJ_2 was not characterized by a good behaviour under negative turnover moments and positive axial loads; neither for the combination of positive turnover moments and negative axial loads. CJ_2 preferential loading conditions can be seen in Figure 3.9 (a).

In Figure 3.7 (b), it can be seen the P_{max} response of BJ_6 as function of the applied axial load and turnover moment. Regarding lowest peak contact pressures (< 90 MPa) in this figure it can be seen that the loading conditions affect a lot BJ_6 performance for loading distribution. BJ_6 had fewer load conditions where this condition was met, and the transition was more abrupt. In this figure can be seen that, in the range of the analysed loading conditions, BJ_6 behaves well under positive turnover moments and positive axial loads, where most of the pressure values under 90 MPa can be found. Regarding to the negative axial loads, BJ_6 does not support this kind of loads. This unstable response to axial loads makes notorious the asymmetry in the sagittal plane of this joint. BJ_6 preferential loading conditions can be seen in Figure 3.9 (b).

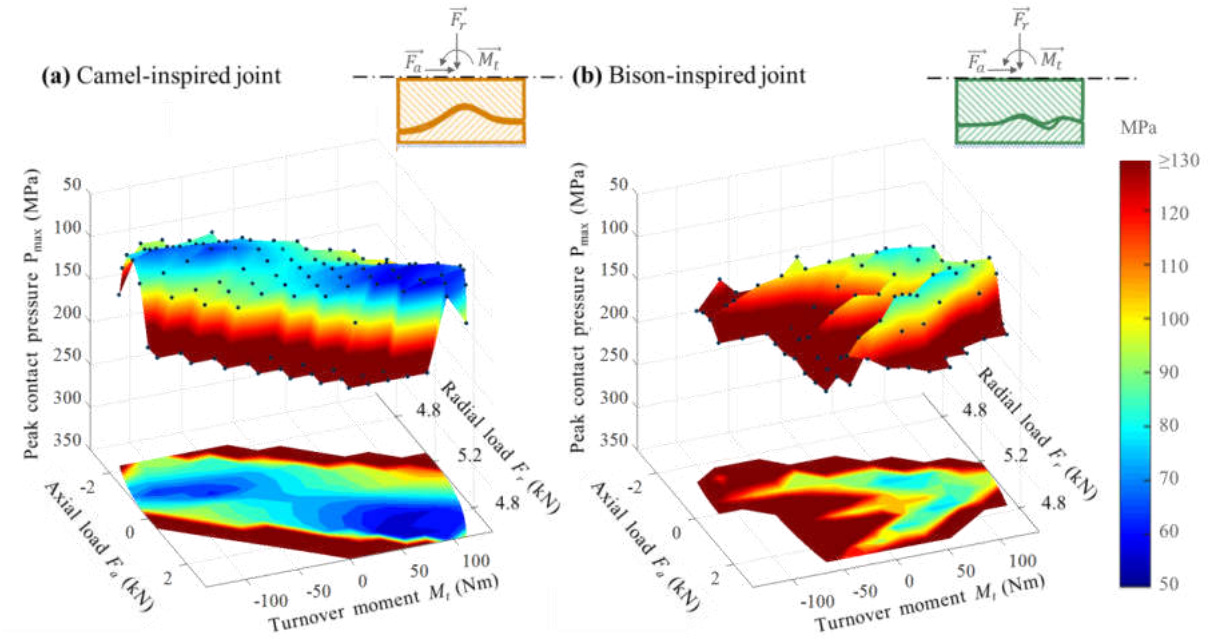

Figure 3.7: Peak contact pressure (in MPa) as a function of the applied axial load (in kN) (radial load as secondary axis (in kN)) and turnover moment (in Nm) for the CJ_2 on the left-hand side and for the BJ_6 on the right-hand side. The colour bar shows also the peak contact pressure values from 50 MPa (in blue colour) to ≥ 130 MPa (in dark red colour).

The comparison of results of two joints under different loading condition and their response can be seen in Figure 3.8. In 37 % of the analysed cases, CJ_2 had lower peak contact pressure with respect to the BJ_6, with a mean difference of 58 %. In 6 % of the cases BJ_6 had lower peak contact pressure regarding to the CJ_2, with a mean difference of 12 %. In 20% of the cases, BJ_6 did not converge while CJ_2 did. In 15% of the cases CJ_2 did not converge while BJ_6 did. Under the analysed loading conditions in 22% of the cases finite element solutions did not converge for any of the joints. In addition to having a lower peak contact pressure CJ_2, it also had a wider load range (the simulations converged in more cases) and with a greater mean difference in pressure than BJ_6. A study which compared different morphologies of elbow implants, showed a good response in terms of load transmission of hourglass-type implant (similar to camel-inspired joint) [62].

F_r (kN)	4.886	5.023	5.121	5.180	5.200	5.180	5.121	5.023	4.886	4.713	4.503
F_a (kN)	-1.779	-1.346	-0.903	-0.453	0.000	0.453	0.903	1.346	1.779	2.198	2.600
M_t (Nm)											
F_r*(-26.5)	100.0	100.0	120.4	62.7	100.0	100.0					
F_r*(-22.1)	100.0	100.0	134.2	73.2	39.6	100.0	100.0				
F_r*(-17.7)	100.0	100.0	75.6	89.5	26.6	85.0	100.0	100.0	100.0		
F_r*(-13.3)	26.6	100.0	100.0	113.1	17.3	87.2	100.0	100.0	100.0	100.0	100.0
F_r*(-8.8)	43.4	100.0	100.0	96.4	25.4	75.1	134.9	8.9	100.0	100.0	100.0
F_r*(-4.4)	100.0	100.0	100.0	28.3	28.1	60.7	120.2	37.7	100.0	100.0	100.0
F_r*(0)		100.0	100.0	18.5	39.4	44.5	97.6	31.0	112.7	100.0	100.0
F_r*(4.4)			100.0	8.3	8.2	57.4	42.5	106.6	16.9	10.0	100.0
F_r*(8.8)			100.0	2.9	16.7	14.0	50.8	47.0	35.6	79.3	49.3
F_r*(13.3)				100.0	17.9	12.3	40.0	21.6	64.1	239.1	100.0
F_r*(17.7)					17.7	9.7	2.6	15.0	173.3	100.0	100.0
F_r*(22.1)					10.1	7.1	1.9	41.6	100.0	100.0	100.0
F_r*(26.5)						12.3	7.0	100.0	100.0	100.0	100.0

Figure 3.8: Comparison of results under different loading conditions. Light green colour BJ_6 had lower P_{max}; light orange colour CJ_2 had lower P_{max}; dark green CJ_2 did not converge; dark orange BJ_6 did not converge; white colour none of the joints did converge.

In Figure 3.9 the contact pressure distribution along the shaft parts of the CJ_2 and BJ_6 can be seen from the bottom view under their preferential loading conditions. On the left-hand side of the Figure 3.9(a) the contact pressure of the CJ_2 with the preferential loading conditions can be seen. On the right-hand side (Figure 3.9 (b)) the contact pressure for the BJ_6 can be seen. The absolute minimum pressure value was found on the CJ_2, with a value of 55 MPa. Under these conditions the resultant load is ubicated at 18 mm to the left from the centre. The contact under these conditions is characterized by two contact zones, with one larger than the other. The minimum value of BJ_6 was of 76 MPa. Under these conditions the resultant load is ubicated at 13 mm to the left from the centre. The contact under these conditions is characterized by three contact zones, two large and one more narrow.

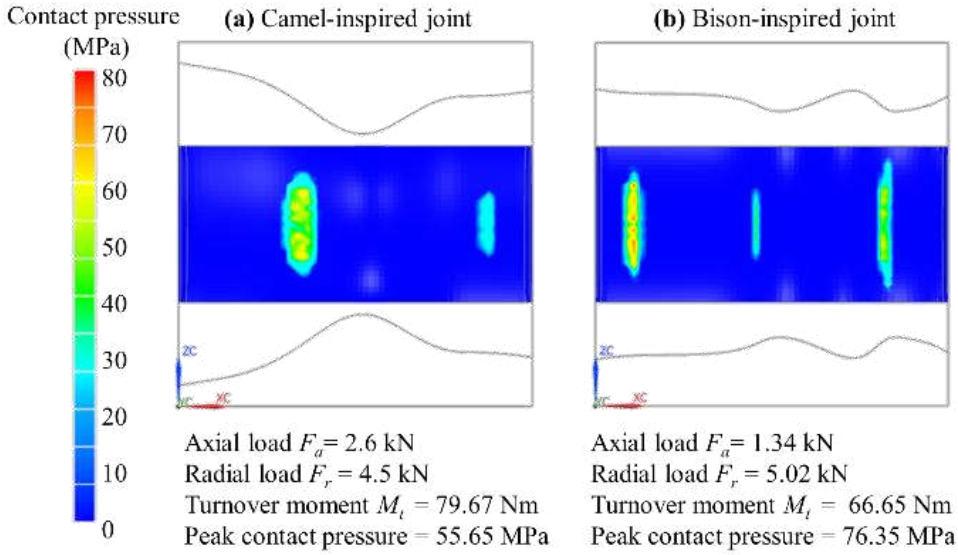

Figure 3.9: Contact pressure under the preferential loading conditions for the (a) CJ_2 and (b) BJ_6. The colour bar represents the contact pressure value from 0 MPa (in blue colour) to 80 MPa (in red colour).

In Figure 3.3, Figure 3.6 and Figure 3.9 it has been seen that the capitellotroclear sulcus deepest part does not transmit loads. In human anatomy this gap may be for the passage of brachial artery, vein and muscle as seen in Figure 3.10. Also, in these figures it is seen that the contact area between trochlea and capitellum is different in both joints. The contact area in general is wider in the capitellum and more extensive in the camel-inspired joint. The contact area in the capitellum is more adequate for axial and radial load transmission respect to the trochlea due to its larger radius of curvature. At the same time trochlea is responsible for providing stability to the applied to turnover moments.

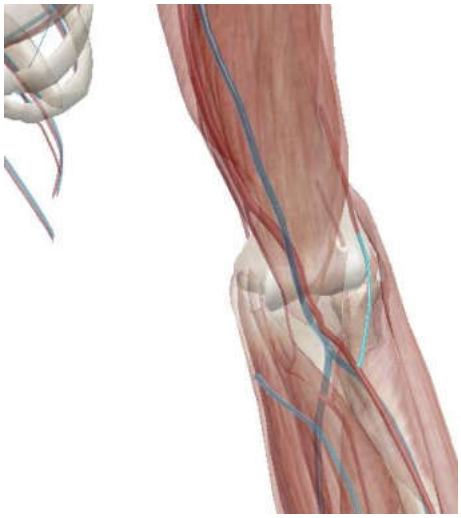

Figure 3.10: Frontal view of the human left elbow with attenuated brachial muscle, brachial artery and brachial vein. [Extracted from Human Anatomy Atlas]

The obtained preferential loading conditions indicated that conditions should be close to the physiological loading conditions. To verify that the obtained results are similar to the real ones, studies on carrying angle in human elbow have been researched. It was found that in a human elbow the carrying angle is not perpendicular, it has 11-16° of medial-lateral inclination, as seen in Figure 3.11 [63].

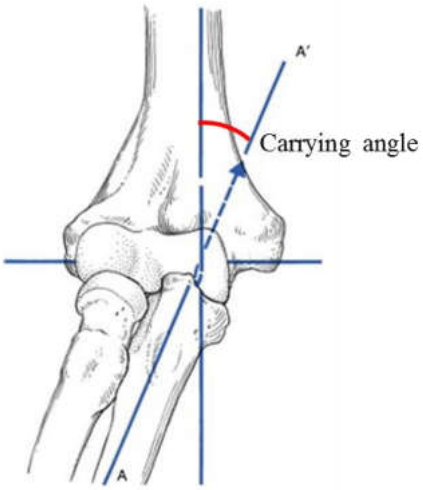

Figure 3.11: Elbow carrying angle. [63]

According to the obtained results preferential loading conditions were positioned as well on medial-lateral loading (camel 30° and bison 15°). This suggests that the obtained as preferential loading conditions should be close to the physiological loading conditions and in quadruped mammals, as in humans, the carrying angle is not perpendicular. In Figure 3.12 can be seen the interpretation of the physiological loading conditions in left elbow of camel and bison.

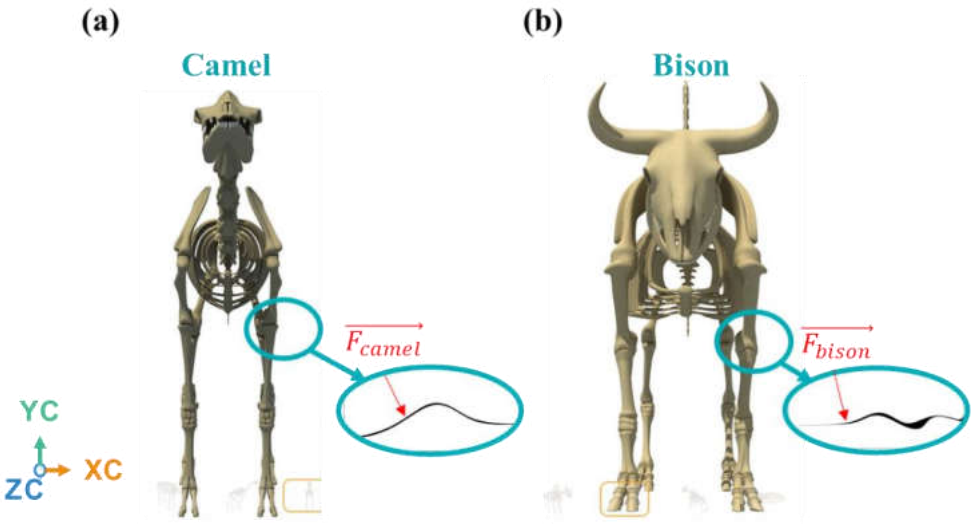

Figure 3.12: Deduced physiological loading conditions in the left elbow of (a) camel; (b) bison. [Extracted from TURBOSQUID]

Chapter 4. Conclusions and future outlook

In this section, first, the obtained conclusions and future outlooks during the project related with the research are presented. Secondly, an evaluation of the developed tasks, acquired knowledge and competences in relation to the university studies will be carried out. In third place, the contributions of the internships to learning will be identified. Finally, the new products, business units or developments that could derive from the TFM will be presented.

A lo largo de este apartado, primero, se van a presentar las conclusiones más concretas sobre lo logrado a lo largo del proyecto y líneas futuras en relación a la investigación. En segundo lugar, se realizará una valoración de las tareas desarrolladas con los conocimientos y competencias adquiridos en relación con los estudios universitarios. En tercer lugar, se identificarán las aportaciones que, en materia de aprendizaje, han supuesto las prácticas. Por último, se presentará los nuevos productos, unidades de negocio o desarrollos que pudieran derivarse del TFM.

Atal honetan, lehenengo, proiektuan ikerketaren inguruan lortutako ondorio zehatzak aurkeztuko dira eta etorkizuneko ildoak. Bigarrenik, egindako lanen balorazioa egingo da, unibertsitate-ikasketekin lotuta eskuratutako ezagutzak eta gaitasunak. Hirugarrenik, praktikek ikaskuntzaren arloan ekarri dituzten ekarpenak identifikatuko dira. Azkenik, TFMtik erator daitezkeen produktu, negozio-unitate edo garapen berriak aurkeztuko dira.

Throughout this work by means of bioinspiration, the different morphologies of biological joints have been used for the design of bio-inspired mechanical joints. Thanks to the correct planning of the tasks and their realization all the objectives and sub-objectives of this project have been achieved. The main objectives of this study have been to evaluate the load bearing performance of the two morphologies proposed by Nature for the hinge joint, to identify their preferential loading conditions and to establish a comparison between the bearing performance of the two morphologies.

Overcoming the challenges presented throughout this project in an autonomous way has helped the student to acquire both technical and professional skills. This section presents the conclusions obtained throughout the project and future lines of this research line identified by the student.

A lo largo de este trabajo mediante la bio-inspiración se han utilizado las distintas morfologías de articulaciones biológicas para el diseño de articulaciones mecánicas bioinspiradas. Gracias a la correcta planificación de las tareas y su realización todos los objetivos y subobjetivos de este proyecto han sido cumplidos. Los objetivos principales de este estudio han sido: evaluar el comportamiento de carga de las dos morfologías propuestas por la Naturaleza para la articulación de bisagra, identificar sus condiciones de carga preferenciales y establecer una comparación entre el rendimiento de carga de las dos morfologías.

Superar los desafíos que se presentaban a lo largo de este proyecto de forma autónoma, ha ayudado a la estudiante a adquirir aptitudes tanto técnicas como profesionales. A lo largo de esta sección se presentan las conclusiones obtenidas a lo largo del proyecto y líneas futuras de investigación identificadas por la estudiante.

Lan honetan zehar, bio-inspirazioaren bidez artikulazio biologikoen morfologia desberdinak erabili dira artikulazio mekaniko bioinspiratuak diseinatzeko. Zereginak behar bezala planifikatzeari eta gauzatzeari esker, proiektu honen helburu eta azpihelburu guztiak bete dira. Azterlan honen helburu nagusiak hauek izan dira: naturak bisagra artikulatzeko proposatutako bi morfologien karga-errendimenduaren abantailak ebaluatzea, lehentasunezko karga-baldintzak identifikatzea eta bi morfologien arteko karga-errendimendua alderatzea.

Proiektu honetan agertzen ziren erronkak modu autonomoan gainditzeak gaitasun teknikoak eta profesionalak eskuratzen lagundu dio ikasleari. Atal honetan, proiektuan zehar lortutako ondorioak eta ikasleak identifikatutako etorkizuneko ikerketa-ildoak aurkezten dira.

4.1. Conclusions of the research

In this study, the finite element method was used to evaluate contact response of two bio-inspired joints under application of external loading. The bio-inspired mechanical joints, created from the camel and bison elbow morphologies, produce different response in terms of load transmission. From the obtained results, it was concluded that camel-inspired joint is more suitable for supporting external combined loads (axial load, radial load and turnover moment). The camel-inspired joint has better load bearing performance (lower peak contact pressures) to combined loads regarding the bison-inspired joint due to its more congruent geometry. It is believed that the lower radius-mass ratio of bison-inspired joint could make it to perform better at high speeds than camel-inspired joint. Future work is required to validate this hypothesis.

For this study, soft tissues were not considered and only the influence of the morphology in load transmission was analysed. Soft tissues (muscles, ligament and tendons) generate an intricate structure that helps to transmit loads and absorb impacts. So, it is believed that soft tissues could actuate more in bison than in camel to help with the load transmission. Future work is required to validate this hypothesis and to highlight the qualities and specialties of bison-inspired joint.

It has been observed that the deepest part of the capitellotrochlear sulcus does not transmit loads. This has been interpreted as a gap for the passage of soft tissues. From the pressure distribution results it has been thought that trochlea and capitellum play a different role in load transmission. It is believed that the main role of the capitellum is to transmit radial and axial loads, while trochlea assists in the transmission of turnover moments.

During this study it has been seen that the morphology of the articular surface variates along the radial direction, changing the contact area during flexion-extension of the elbow. From the performed contact simulations with bio-inspired joints of the same group, slightly different results were obtained for each joint. The results suggested that according to the flexion-extension angle the load is differently transmitted and the preferential loading conditions may vary. For future work, it is considered interesting to analyse the load bearing performance by reusing the morphological geometry of the articular surfaces to evaluate their response, including cartilage.

The geometrical asymmetry with respect to mid-sagittal plane of the bison-inspired joints is reflected in their load bearing response. This group of joints showed a better pressure distribution under positive turnover moments. Negative turnover moments generate higher

contact pressures. Additionally, the larger coverage intervals of peak contact pressures obtained from the negative turnover moments can be interpreted as an instability. This instability may be caused by the own geometry of the joint. As it has been seen this instability can cause edge effects and reduce durability of the joints. This suggests that the obtained as preferential loading conditions should be close to the physiological loading conditions. According to the obtained results, preferential loading conditions were positioned as well on medial-lateral loading (bison 15° of inclination). In conclusion, the bison-inspired joint transmits better positive axial loads and positive turnover moments when loads are applied in a constant way. The loads during operation of this joint must be constant because a slight variation may generate an overpressure.

In quadrupedal mammals, nature has created two different morphologies (two bumps and three bumps) for the elbow joints, even if these joints have the same kinematic requirements (same DOF). This study showed that the response in terms of load transmission for the two morphologies is different. The preferential loading conditions for each of these morphologies were determined and camel-inspired joint (two bumps morphology) had the best load bearing performance. The obtained results can be interesting for the design of mechanical elements for industrial applications or biomedical implants for biological applications.

4.2. Valuation of the developed tasks and acquired skills related with the chosen competences

According to the objectives of the project, the following three competences were chosen to be acquired during the development of the project:

- To show personal and technical capacity in an autonomous development of the End of Degree Project within a teamwork environment. To justify the conclusions and scope of the results obtained.
- To take the initiative in problem solving, decision making and creativity, and to communicate and share knowledge and skills, understanding the ethical and professional responsibilities of the business activity in the field of Biomedical Engineering.
- To know how to perform measurements, calculations, valuations, studies, reports, task planning schemes, and other activities pertaining to the field of Biomedical Engineering.

In November, when the project began, the student was informed about the research area in which the study was going to be carried out. It was presented to the student the available material, the requirements and the objective to achieve during the project. From there, the student had to work autonomously with help of the tutor and other members of the team experts in different areas. The student had to determine the precise subject of the study, define the tasks to be carried out and do the tasks planning of the eight-month project.

During this project, the student often had to work autonomously and then share the knowledge, obtained conclusions or the performed tasks with the team, demonstrating communication skills. The student also had to take charge of the initiative and make decisions regarding the research, assuming responsibilities. To carry out these tasks the student had to show several aptitudes such as seriousness, responsibility and dedication. In addition, the project required a high level of creativity and effort to overcome the challenges encountered throughout the project.

In the middle of the project the student had to return to the home country because of the health alert for COVID-19. The developed tasks were affected and difficult because of lack of access to the software and simulations. During this time the writing of the article and the document was carried out and the follow up was done through videoconferences via skype twice a week. Once the university was opened again the material could be retrieved and the simulations were finished telematically by videoconferences.

At the end of the project the student had to present a report and make a presentation to defend the project. In the report the student had to justify the conclusions and scope of the obtained results in a clearly and concisely. Therefore, regarding the selected competences, the activities carried out during the development of the project have helped the student to acquire these competences.

4.3. Identify the contributions in learning material acquired during this project

Different tasks carried out during the project forced the student to acquire a series of aptitudes and skills in learning material. Following can be seen these aptitudes:

- Plan, develop and supervise a scientific research.

- Design bio-inspired mechanical joints using CAD software CATIA V5.
- Design simulation protocol.
- Develop macro VBA to automatize the process.
- Carry out simulation protocol.
- Treat and analyse simulation results.

4.4. New products, business models or developments that may derive from this project

Although the results obtained from the numerical simulations, as well as the pressure distribution surface, seem promising, there is still room for verification and validation of these results. As results were only obtained from numerical models the following step would be the implementation of an experimental protocol to verify these results.

For an accurate estimation of load transmission in a biological joint a musculoskeletal modelling should be created. Even if some biomechanical models have been built with different animals to study their locomotion as horse, sheeps and seahorse there are many others that have not been built jet. First step would be the characterization of the biomechanical relevant features of these animals, that have not been described jet in literature. Second step would be their biomechanical modelling constructions. By incorporating bone cartilage into the musculoskeletal model, even more precise results would be obtained.

Also is important to evaluate the real advantage of bio-inspired mechanical joints over current joints. For this a comparison should be made of contact distribution and the peak contact pressure of these joints. This would validate and further strengthen the design of mechanical joints using bioinspiration.

In addition, as it has been seen, the modification of the geometry can cause great changes in the pressure distribution. Therefore, a possible optimization of the revolution profile of the mechanical joint could be done. Through this optimization best peak contact pressure distribution could be achieved. In this way, the geometry could also be modified to particular application loading conditions that the mechanical joint will support during the service life.

In addition, it is considered that this project could lead to the submission of a scientific article to a journal. To be precise, the results of this work are expected to be published in the

Journal of Bioinspiration & Biomimetics (Engineering, multidisciplinary – SCIE), that belongs to IOP Publishing and had an impact factor of 3.130 in year 2018 and belonged to a quartile of Q1. This journal publishes research that discovers and uses principles from natural systems to create physical models, engineering systems and technological designs.

With all that has been said so far, it remains to conclude that this project is expected to revolutionize the design of sliding contact bearings. In the not-so-distant future, it is expected that the design of sliding contact bearings will change from cylinders to more complex geometries. It is also expected that these complex geometries extend bearings lifespan and reduce the current failures problems caused by wear appearing due to misalignment between inner and outer races of the bearings.

Chapter 5. Economic memory of the project

During the development of the project, the student received support and help from different parts of the responsible and not responsible personnel. The provided service by the personnel and the required equipment supposed a series of economic costs. All these incomes and costs have been registered with the objective of estimating the total economic cost of the project.

Table 5.1 shows the estimation of the economics cost of the project. First different economic compensations, incomes, are presented. Outcomes are presented in second place, the cost per hour of different involved personal, and in third place, costs of different softwares used during the project.

Table 5.1: Economic cost estimation of the project.

TYPE OF GRANT	Income per month (€/month)	Months	Total income (€)
Erasmus +	350	3	1 050
Aix-Marseille Université	416.25	8	3 330
INVOLVED PERSONAL	Cost per hour (€/hour)	Spent hours	Total cost (€)
Pedro A.	90	10	900
Santiago A.	87.29	150	13 093.5
Jean-Marc L.	133.49	20	2 669.8
Dimitrios B.	87.29	100	8 729
Workshop Team	59.68	30	1 790.4
USED SOFTWARE	Cost per month (€/month)	Months	Total cost (€)
NX licence	500	8	4 000
TOTAL COST OF THE PROJECT			**35 562.7 €**

Chapter 6. Personal evaluation of the internship and Final Degree Project

During this section the personal evaluation of the trainee is presented about the internship program and the tasks carried out during the final degree project. An evaluation of the practices carried out and suggestion for improvement are made

I believe that the opportunity to do the internship abroad has provided me with a great opportunity to develop both personally and professionally. Working in a research team has helped me to confirm my future job preferences and to acquire very important knowledge for my professional future. I have to thank the opportunity of doing the final degree project abroad to the Erasmus+ program and to the received help along these months by the host university Aix-Marseille Université.

The opportunity to do the internship in France has helped me with the improvement of this language. Being in a foreign country, with a language other than my mother tongue, has helped me to trust myself and to get rid of the fear of speaking foreign languages.

The best part of the internship was the information and literature researching and conclusions contrast. Although the experience in general has been magnificent, I would also have liked to carry out the experimental validation which, due to the situation of COVID 19, could not have been done in time. The internships almost fulfilled all my expectations, but I feel like I did not get tutoring as much as I expected, and this could have slowed down the development of the project.

Living eight months away from home is not something that everyone can afford. Except for that reason, I recommend everyone who can live this experience not to hesitate to experience it. The experience you acquire, the network of contacts you generate are just some examples of the things you gain through this experience.

Appendices

Appendix A

Codes of the macro VBA for automatic simulation generation and calculation

```
' ====================================================================
' NX 11.0.0.33
' Journal created by serveur2 on Fri Jan 10 08:11:29 2020 Paris, Madrid
'
' Written by Aliona Sanz Idirin (Also containing algorith from automatic
generation with NX)
' Aix-Mareseille Universite / ISM-CBI
' 2020/03/10

' This is one of the codes for the automatic solution creation and calculation.
' Simulations are automatically created under defined conditions and their
results are solved on a file

Imports System
Imports NXOpen
Imports System.IO 'nuevo

Module NXJournal
Public pi as Double

Sub Main (ByVal args() As String)
pi=4*Math.atan(1)

Dim FileRoute As String =
"C:\Users\serveur2\Documents\Aliona\VB_automatization\solving_parameters.txt" '
Input of the conditions table to simulate
Dim File As New StreamReader(FileRoute)

' Variables declaration
Dim Moment As Double = 0 ' Turnover moment conditions of the simulation
Dim forceInclinationAngle As Double = 0 ' Axial load inclination angle
Dim forceMagnitud1 As Double=0 ' Magnitude of the load applied on the first node
Dim forceMagnitud2 As Double=0 ' Magnitude of the load applied on the third node
Dim FMax As Integer = 5200 ' Maximum load to be applied
Dim l As Double = 0.115 ' Distance to the external nodes
Dim index As Integer ' For solution solving'
index=0
Dim theSession As NXOpen.Session = NXOpen.Session.GetSession()
Dim workSimPart As NXOpen.CAE.SimPart = CType(theSession.Parts.BaseWork,
NXOpen.CAE.SimPart)
Dim displaySimPart As NXOpen.CAE.SimPart = CType(theSession.Parts.BaseDisplay,
NXOpen.CAE.SimPart)
Dim simPart1 As NXOpen.CAE.SimPart = CType(workSimPart, NXOpen.CAE.SimPart)
Dim simSimulation1 As NXOpen.CAE.SimSimulation = Nothing
simSimulation1 = simPart1.Simulation
Dim simSolution1 As NXOpen.CAE.SimSolution = Nothing
Dim psolutions1(121) As NXOpen.CAE.SimSolution 'number of solutions or more'
Dim modelingObjectPropertyTable1 As NXOpen.CAE.ModelingObjectPropertyTable =
CType(workSimPart.ModelingObjectPropertyTables.FindObject("SsmoPropTable[Structu
ral Linear Output Requests1]"), NXOpen.CAE.ModelingObjectPropertyTable)
Dim propertyTable1 As NXOpen.CAE.PropertyTable = Nothing
Dim setManager1 As NXOpen.CAE.SetManager = Nothing
Dim setManager2 As NXOpen.CAE.SetManager = Nothing
Dim setManager3 As NXOpen.CAE.SetManager = Nothing
Dim setManager4 As NXOpen.CAE.SetManager = Nothing
Dim setManager5 As NXOpen.CAE.SetManager = Nothing
Dim setManager6 As NXOpen.CAE.SetManager = Nothing
Dim setManager7 As NXOpen.CAE.SetManager = Nothing
Dim setManager8 As NXOpen.CAE.SetManager = Nothing
Dim setManager9 As NXOpen.CAE.SetManager = Nothing
```

```
Dim setManager10 As NXOpen.CAE.SetManager = Nothing
Dim setManager11 As NXOpen.CAE.SetManager = Nothing
Dim setManager12 As NXOpen.CAE.SetManager = Nothing
Dim setManager13 As NXOpen.CAE.SetManager = Nothing
Dim setManager14 As NXOpen.CAE.SetManager = Nothing
Dim setManager15 As NXOpen.CAE.SetManager = Nothing
Dim setManager16 As NXOpen.CAE.SetManager = Nothing
Dim setManager17 As NXOpen.CAE.SetManager = Nothing
Dim setManager18 As NXOpen.CAE.SetManager = Nothing
Dim setManager19 As NXOpen.CAE.SetManager = Nothing
Dim setManager20 As NXOpen.CAE.SetManager = Nothing
Dim setManager21 As NXOpen.CAE.SetManager = Nothing
Dim setManager22 As NXOpen.CAE.SetManager = Nothing
Dim markId3 As NXOpen.Session.UndoMarkId = Nothing
Dim markId4 As NXOpen.Session.UndoMarkId = Nothing
Dim markId5 As NXOpen.Session.UndoMarkId = Nothing
Dim setManager23 As NXOpen.CAE.SetManager = Nothing
Dim setManager24 As NXOpen.CAE.SetManager = Nothing
Dim setManager25 As NXOpen.CAE.SetManager = Nothing
Dim setManager26 As NXOpen.CAE.SetManager = Nothing
Dim setManager27 As NXOpen.CAE.SetManager = Nothing
Dim setManager28 As NXOpen.CAE.SetManager = Nothing
Dim setManager29 As NXOpen.CAE.SetManager = Nothing
Dim setManager30 As NXOpen.CAE.SetManager = Nothing
Dim setManager31 As NXOpen.CAE.SetManager = Nothing
Dim setManager32 As NXOpen.CAE.SetManager = Nothing
Dim setManager33 As NXOpen.CAE.SetManager = Nothing
Dim setManager34 As NXOpen.CAE.SetManager = Nothing
Dim setManager35 As NXOpen.CAE.SetManager = Nothing
Dim setManager36 As NXOpen.CAE.SetManager = Nothing
Dim setManager37 As NXOpen.CAE.SetManager = Nothing
Dim setManager38 As NXOpen.CAE.SetManager = Nothing
Dim setManager39 As NXOpen.CAE.SetManager = Nothing
Dim setManager40 As NXOpen.CAE.SetManager = Nothing
Dim setManager41 As NXOpen.CAE.SetManager = Nothing
Dim setManager42 As NXOpen.CAE.SetManager = Nothing
Dim setManager43 As NXOpen.CAE.SetManager = Nothing
Dim setManager44 As NXOpen.CAE.SetManager = Nothing
Dim nErrs1 As Integer = Nothing
Dim markId8 As NXOpen.Session.UndoMarkId = Nothing
Dim propertyTable2 As NXOpen.CAE.PropertyTable = Nothing
Dim id1 As NXOpen.Session.UndoMarkId = Nothing
Dim nErrs2 As Integer = Nothing
Dim simSolutionStep1 As NXOpen.CAE.SimSolutionStep = Nothing
Dim nErrs3 As Integer = Nothing
Dim markId9 As NXOpen.Session.UndoMarkId = Nothing
Dim simSimulationObject1 As NXOpen.CAE.SimSimulationObject =
CType(simSimulation1.SimulationObjects.FindObject("SimulationObject[Face
Contact(1)]"), NXOpen.CAE.SimSimulationObject)'add face contact'
Dim markId10 As NXOpen.Session.UndoMarkId = Nothing
Dim simConstraint1 As NXOpen.CAE.SimConstraint =
CType(simSimulation1.Constraints.FindObject("Constraint[Fixed(1)]"),
NXOpen.CAE.SimConstraint)'add restriction fixed to the ground'
Dim markId11 As NXOpen.Session.UndoMarkId = Nothing
Dim simConstraint2 As NXOpen.CAE.SimConstraint =
CType(simSimulation1.Constraints.FindObject("Constraint[UserDefined(1)]"),
NXOpen.CAE.SimConstraint)'add restriction node 2'
Dim propertyTable3 As NXOpen.CAE.PropertyTable = Nothing
Dim setManager45 As NXOpen.CAE.SetManager = Nothing
Dim unit1 As NXOpen.Unit =
CType(workSimPart.UnitCollection.FindObject("Degrees"), NXOpen.Unit)
Dim vector1 As NXOpen.Vector3d= New NXOpen.Vector3d()
Dim origin1 As NXOpen.Point3d = New NXOpen.Point3d(0.0, 0.0, 0.0)
Dim direction1 As NXOpen.Direction = Nothing
```

```
Dim fEModelOccurrence1 As NXOpen.CAE.FEModelOccurrence =
CType(workSimPart.FindObject("FEModelOccurrence[1]"),
NXOpen.CAE.FEModelOccurrence)
Dim fENode1 As NXOpen.CAE.FENode = CType(fEModelOccurrence1.Find("Node[1]"),
NXOpen.CAE.FENode)'node 1'
Dim objects1(0) As NXOpen.CAE.SetObject
Dim unit2 As NXOpen.Unit =
CType(workSimPart.UnitCollection.FindObject("Newton"), NXOpen.Unit)
Dim expression1 As NXOpen.Expression = Nothing
Dim fieldManager1 As NXOpen.Fields.FieldManager =
CType(workSimPart.FindObject("FieldManager"), NXOpen.Fields.FieldManager)
Dim scalarFieldWrapper1 As NXOpen.Fields.ScalarFieldWrapper = Nothing
Dim simBC1 As NXOpen.CAE.SimBC = Nothing
Dim propertyTable4 As NXOpen.CAE.PropertyTable = Nothing
Dim setManager46 As NXOpen.CAE.SetManager = Nothing
Dim objects2(0) As NXOpen.CAE.SetObject
Dim fENode2 As NXOpen.CAE.FENode = CType(fEModelOccurrence1.Find("Node[3]"),
NXOpen.CAE.FENode)'node 3'
Dim expression2 As NXOpen.Expression = Nothing
Dim scalarFieldWrapper2 As NXOpen.Fields.ScalarFieldWrapper = Nothing
Dim simBC2 As NXOpen.CAE.SimBC = Nothing
Dim propertyTable8 As NXOpen.CAE.PropertyTable = Nothing
Dim theSimSolveManager As NXOpen.CAE.SimSolveManager =
NXOpen.CAE.SimSolveManager.GetSimSolveManager(theSession)
Dim numsolutionssolved1 As Integer = Nothing
Dim numsolutionsfailed1 As Integer = Nothing
Dim numsolutionsskipped1 As Integer = Nothing
Dim skipSolutionsWithResult As Boolean
Dim anyPartsModified1 As Boolean = Nothing
Dim partSaveStatus1 As NXOpen.PartSaveStatus = Nothing

While File.Peek <> -1

        Dim FileLine As String = File.ReadLine.ToString
        Moment = Mid(FileLine, 1, 7).Trim
        forceMagnitud2 = (-cstr(Moment)/l + FMax)/2
        forceMagnitud1 = FMax - forceMagnitud2
        forceInclinationAngle = Mid(FileLine, 8, FileLine.Length - 1).Trim
        '-----------------
        'Create simulation
        '-----------------
        simSolution1 = simSimulation1.CreateSolution("SAMCEF", "Structural",
"Linear Static Analysis",
"Solution_"&cstr(forceInclinationAngle)&"°_F1_"&cstr(forceMagnitud1)&"N_F2_"&cst
r(forceMagnitud2)&"N", NXOpen.CAE.SimSimulation.AxisymAbstractionType.None)'Name
of solution'
        propertyTable1 = modelingObjectPropertyTable1.PropertyTable
        setManager1 = propertyTable1.GetSetManagerPropertyValue("Shear Forces
Moments - Group")
        setManager2 = propertyTable1.GetSetManagerPropertyValue("Normal Forces
Moments - Group")
        setManager3 = propertyTable1.GetSetManagerPropertyValue("Linear Stress
Tensor - Group")
        setManager4 = propertyTable1.GetSetManagerPropertyValue("Normal Stress
Beams Rods - Group")
        setManager5 = propertyTable1.GetSetManagerPropertyValue("Shear Stress
Beams - Group")
        setManager6 = propertyTable1.GetSetManagerPropertyValue("VonMises
Equivalent Stress - Group")
        setManager7 = propertyTable1.GetSetManagerPropertyValue("Total Strain
Tensor - Group")
        setManager8 = propertyTable1.GetSetManagerPropertyValue("Composite Stress
Tensor - Group")
```

```
        setManager9 = propertyTable1.GetSetManagerPropertyValue("Composite
Interlaminar Stress Tensor - Group")
        setManager10 = propertyTable1.GetSetManagerPropertyValue("Composite
Mechanical Strain Tensor - Group")
        setManager11 = propertyTable1.GetSetManagerPropertyValue("Composite Total
Strain Tensor - Group")
        setManager12 = propertyTable1.GetSetManagerPropertyValue("Composite Tsai-
Hill 1 Criteria - Group")
        setManager13 = propertyTable1.GetSetManagerPropertyValue("Composite Tsai-
Hill 2 Criteria - Group")
        setManager14 = propertyTable1.GetSetManagerPropertyValue("Composite Tsai-
Hill 3 Criteria - Group")
        setManager15 = propertyTable1.GetSetManagerPropertyValue("Composite
Hashin 1 Criteria - Group")
        setManager16 = propertyTable1.GetSetManagerPropertyValue("Composite
Hashin 2 Criteria - Group")
        setManager17 = propertyTable1.GetSetManagerPropertyValue("Composite
Hashin 3 Criteria - Group")
        setManager18 = propertyTable1.GetSetManagerPropertyValue("Composite Full
Hashin Criteria - Group")
        setManager19 = propertyTable1.GetSetManagerPropertyValue("Composite Tsai-
Wu Criteria - Group")
        setManager20 = propertyTable1.GetSetManagerPropertyValue("Composite Puck
Criteria - Group")
        setManager21 = propertyTable1.GetSetManagerPropertyValue("Contact -
Group")'activate contact'
        setManager22 = propertyTable1.GetSetManagerPropertyValue("User Codes -
Group")
        markId3 = theSession.SetUndoMark(NXOpen.Session.MarkVisibility.Invisible,
"Structural Linear Output Requests1")
        markId4 = theSession.SetUndoMark(NXOpen.Session.MarkVisibility.Invisible,
"Structural Linear Output Requests1")
        setManager23 = propertyTable1.GetSetManagerPropertyValue("Shear Forces
Moments - Group")
        setManager24 = propertyTable1.GetSetManagerPropertyValue("Normal Forces
Moments - Group")
        setManager25 = propertyTable1.GetSetManagerPropertyValue("Linear Stress
Tensor - Group")
        setManager26 = propertyTable1.GetSetManagerPropertyValue("Normal Stress
Beams Rods - Group")
        setManager27 = propertyTable1.GetSetManagerPropertyValue("Shear Stress
Beams - Group")
        setManager28 = propertyTable1.GetSetManagerPropertyValue("VonMises
Equivalent Stress - Group")
        setManager29 = propertyTable1.GetSetManagerPropertyValue("Total Strain
Tensor - Group")
        setManager30 = propertyTable1.GetSetManagerPropertyValue("Composite
Stress Tensor - Group")
        setManager31 = propertyTable1.GetSetManagerPropertyValue("Composite
Interlaminar Stress Tensor - Group")
        setManager32 = propertyTable1.GetSetManagerPropertyValue("Composite
Mechanical Strain Tensor - Group")
        setManager33 = propertyTable1.GetSetManagerPropertyValue("Composite Total
Strain Tensor - Group")
        setManager34 = propertyTable1.GetSetManagerPropertyValue("Composite Tsai-
Hill 1 Criteria - Group")
        setManager35 = propertyTable1.GetSetManagerPropertyValue("Composite Tsai-
Hill 2 Criteria - Group")
        setManager36 = propertyTable1.GetSetManagerPropertyValue("Composite Tsai-
Hill 3 Criteria - Group")
        setManager37 = propertyTable1.GetSetManagerPropertyValue("Composite
Hashin 1 Criteria - Group")
        setManager38 = propertyTable1.GetSetManagerPropertyValue("Composite
Hashin 2 Criteria - Group")
```

```
        setManager39 = propertyTable1.GetSetManagerPropertyValue("Composite
Hashin 3 Criteria - Group")
        setManager40 = propertyTable1.GetSetManagerPropertyValue("Composite Full
Hashin Criteria - Group")
        setManager41 = propertyTable1.GetSetManagerPropertyValue("Composite Tsai-
Wu Criteria - Group")
        setManager42 = propertyTable1.GetSetManagerPropertyValue("Composite Puck
Criteria - Group")
        setManager43 = propertyTable1.GetSetManagerPropertyValue("Contact -
Group")
        setManager44 = propertyTable1.GetSetManagerPropertyValue("User Codes -
Group")
        markId8 = theSession.SetUndoMark(NXOpen.Session.MarkVisibility.Invisible,
Nothing)
        propertyTable2 = simSolution1.PropertyTable
        propertyTable2.SetNamedPropertyTablePropertyValue("Output Requests",
modelingObjectPropertyTable1)
        id1 = theSession.NewestVisibleUndoMark
        nErrs2 = theSession.UpdateManager.DoUpdate(id1)
        simSolutionStep1 = simSolution1.CreateStep(0, "Subcase - Static Loads 1")
        simSolution1.ActiveStep = simSolutionStep1
        nErrs3 = theSession.UpdateManager.DoUpdate(markId8)
        theSession.SetUndoMarkName(id1, "Solution")
        '--------------------
        ' Activate constrains
        '--------------------
        markId9 = theSession.SetUndoMark(NXOpen.Session.MarkVisibility.Visible,
"Add to active solution or step")
        simSolution1.AddBc(simSimulationObject1)
        markId10 = theSession.SetUndoMark(NXOpen.Session.MarkVisibility.Visible,
"Add to active solution or step")
        simSolution1.AddBc(simConstraint1)
        markId11 = theSession.SetUndoMark(NXOpen.Session.MarkVisibility.Visible,
"Add to active solution or step")
        simSolution1.AddBc(simConstraint2)
        '------------------------------------------------
        ' Create force dependent to the variable angle
        '------------------------------------------------
        theSession.Preferences.Modeling.UpdatePending = False
        Dim simPart2 As NXOpen.CAE.SimPart = CType(workSimPart,
NXOpen.CAE.SimPart)
        Dim simSimulation2 As NXOpen.CAE.SimSimulation = Nothing
        ' NODE 1
        simSimulation2 = simPart2.Simulation
        Dim simBCBuilder1 As NXOpen.CAE.SimBCBuilder = Nothing
        simBCBuilder1 =
simSimulation2.CreateBcBuilderForLoadDescriptor("magnitudeDirectionForce",
"N1_F1_"&cstr(forceMagnitud1)&"N_"&cstr(forceInclinationAngle)&"°", 1)'Name of
first load'
        propertyTable3 = simBCBuilder1.PropertyTable
        setManager45 = simBCBuilder1.TargetSetManager
        vector1.X=Math.cos(forceInclinationAngle*pi/180)
        vector1.Y=Math.sin(forceInclinationAngle*pi/180)
        vector1.Z=0.0
        direction1 = workSimPart.Directions.CreateDirection(origin1, vector1,
NXOpen.SmartObject.UpdateOption.AfterModeling)
        direction1.ReverseDirection()
        objects1(0).Obj = fENode1
        objects1(0).SubType = NXOpen.CAE.CaeSetObjectSubType.None
        objects1(0).SubId = 0
        setManager45.SetTargetSetMembers(0, objects1)
        expression1 =
workSimPart.Expressions.CreateSystemExpressionWithUnits(cstr(forceMagnitud1),
unit2)'forceMagnitud'
```

```
        scalarFieldWrapper1 =
fieldManager1.CreateScalarFieldWrapperWithExpression(expression1)
        propertyTable3.SetScalarFieldWrapperPropertyValue("TotalForce",
scalarFieldWrapper1)
        propertyTable3.SetVectorPropertyValue("Local Axis", direction1)
        propertyTable3.SetTablePropertyWithoutValue("DistributionField")
        simBC1 = simBCBuilder1.CommitAddBc()
        simBCBuilder1.Destroy()
        'NODE_3
        theSession.Preferences.Modeling.UpdatePending = False
        Dim simBCBuilder2 As NXOpen.CAE.SimBCBuilder = Nothing
        simBCBuilder2 =
simSimulation2.CreateBcBuilderForLoadDescriptor("magnitudeDirectionForce",
"N3_F2_"&cstr(forceMagnitud2)&"N_"&cstr(forceInclinationAngle)&"°", 1)'Name of
the second load'
        propertyTable4 = simBCBuilder2.PropertyTable
        setManager46 = simBCBuilder2.TargetSetManager
        direction1 = workSimPart.Directions.CreateDirection(origin1, vector1,
NXOpen.SmartObject.UpdateOption.AfterModeling)
        direction1.ReverseDirection()
        objects2(0).Obj = fENode2
        objects2(0).SubType = NXOpen.CAE.CaeSetObjectSubType.None
        objects2(0).SubId = 0
        setManager46.SetTargetSetMembers(0, objects2)
        expression2 =
workSimPart.Expressions.CreateSystemExpressionWithUnits(cstr(forceMagnitud2),
unit2)'forceMagnitud'
        scalarFieldWrapper2 =
fieldManager1.CreateScalarFieldWrapperWithExpression(expression2)
        propertyTable4.SetScalarFieldWrapperPropertyValue("TotalForce",
scalarFieldWrapper2)
        propertyTable4.SetVectorPropertyValue("Local Axis", direction1)
        simBC2 = simBCBuilder2.CommitAddBc()
        simBCBuilder2.Destroy()
        '------------
        ' Save
        '------------
        psolutions1(index) = simSolution1
        index+=1
        theSession.Parts.SaveAll(anyPartsModified1, partSaveStatus1)
        partSaveStatus1.Dispose()

End While
'-------
' Simulate
'-------
propertyTable8 = simSolution1.SolverOptionsPropertyTable
propertyTable8.SetBooleanPropertyValue("Enable Multithreads", True)
propertyTable8.SetIntegerPropertyValue("Solver NTHREADS", 8)
theSimSolveManager.SolveAllSolutions(NXOpen.CAE.SimSolution.SolveOption.Solve,
NXOpen.CAE.SimSolution.SetupCheckOption.DoNotCheck,
NXOpen.CAE.SimSolution.SolveMode.Foreground, skipSolutionsWithResult,
numsolutionssolved1, numsolutionsfailed1, numsolutionsskipped1)
'------------
' Save
'------------
theSession.Parts.SaveAll(anyPartsModified1, partSaveStatus1)
partSaveStatus1.Dispose()
End Sub
End Module
        '
```

==========

```
' ====================================================================
' NX 11.0.0.33
' Journal created by serveur2 on Thu Jan 30 08:56:09 2020 Paris, Madrid
'
' Written by Aliona Sanz Idirin (Also containing algorithm from automatic
generation with NX)
' Aix-Mareseille Universite / ISM-CBI
' 2020/03/10

' This is one of the codes for the average peak contact pressure values
extraction of the simulations. The maximum peak contact pressure is calculated
and the average of the five highest values is calculated and saved in a file.

Imports System
Imports NXOpen
Imports System.IO
Imports System.Runtime.CompilerServices
Imports System.Collections.Generic
Imports NXOpen.UF

Module NXJournal
Sub Main (ByVal args() As String)

Dim theSession As NXOpen.Session = NXOpen.Session.GetSession()'
Dim workSimPart As NXOpen.CAE.SimPart = CType(theSession.Parts.BaseWork,
NXOpen.CAE.SimPart)
Dim displaySimPart As NXOpen.CAE.SimPart = CType(theSession.Parts.BaseDisplay,
NXOpen.CAE.SimPart)'
Dim FileRoute As String =
"C:\Users\serveur2\Documents\Aliona\VB_automatization\solving_parameters.txt"
Dim ParametersFile As New StreamReader(FileRoute)
Dim file = new
System.IO.StreamWriter("C:\Users\serveur2\Documents\Aliona\CAO_Simulations_V5\Re
sultados\Bison_G1_complet.txt",False)
Dim simSimulation1 As NXOpen.CAE.SimSimulation =
CType(workSimPart.FindObject("Simulation"), NXOpen.CAE.SimSimulation)'
Dim resultParameters1 As NXOpen.CAE.ResultParameters = Nothing
resultParameters1 = theSession.ResultManager.CreateResultParameters()
resultParameters1.SetResultComponent(CAE.Result.Component.Scalar)
resultParameters1.SetAbsoluteValue(True)
resultParameters1.SetExcludeElementsNotVisible(True)
Dim forceMagnitud2 As Double=0
Dim FMax As Integer = 5200
Dim l As Double = 0.115
file.WriteLine ("Moment      " & "Angle     " & "Peak contact pressure   ")
Dim file = new
System.IO.StreamWriter("C:\Users\serveur2\Documents\Aliona\CAO_Simulations_V6_Fm
ax5200N\Resultados\Camel2600_G2_max_array.txt",False)

While ParametersFile.Peek <> -1 'Load th solutions one by one
        Dim FileLine As String = ParametersFile.ReadLine.ToString
        Moment = Mid(FileLine, 1, 7).Trim
        forceMagnitud2 = (-cstr(Moment)/l + FMax)/2
        forceMagnitud1 = FMax - forceMagnitud2
        forceInclinationAngle = Mid(FileLine, 8, FileLine.Length - 1).Trim
        markId1 = theSession.SetUndoMark(NXOpen.Session.MarkVisibility.Visible,
"Activate Solution")
        Dim simSolution1 As NXOpen.CAE.SimSolution =
CType(simSimulation1.FindObject("Solution[Solution_"&cstr(forceInclinationAngle)
&"°_F1_"&cstr(forceMagnitud1)&"N_F2_"&cstr(forceMagnitud2)&"N]"),
NXOpen.CAE.SimSolution)'
```

```
        Dim simSolutionStep1 As NXOpen.CAE.SimSolutionStep =
CType(simSolution1.FindObject("SolutionStep[Subcase - Static Loads 1]"),
NXOpen.CAE.SimSolutionStep)
        simSolution1.ActiveStep = simSolutionStep1
        Dim resultManager1 As NXOpen.CAE.ResultManager =
CType(theSession.ResultManager, NXOpen.CAE.ResultManager)
        Dim solresults As NXOpen.CAE.SolutionResult =
resultManager1.CreateSolutionResult(simSolution1)
        Dim results As NXOpen.CAE.Result = CType(solresults, NXOpen.CAE.Result)
        Dim solutionResult1 As NXOpen.CAE.SolutionResult =
CType(resultManager1.FindObject("SolutionResult[Camel_G2_sim1.sim_Solution_"&cst
r(forceInclinationAngle)&"°_F1_"&cstr(forceMagnitud1)&"N_F2_"&cstr(forceMagnitud
2)&"N]"), NXOpen.CAE.SolutionResult)
        Dim loadcase1 As NXOpen.CAE.Loadcase =
CType(solutionResult1.Find("Loadcase[1]"), NXOpen.CAE.Loadcase)
        Dim iteration1 As NXOpen.CAE.Iteration =
CType(loadcase1.Find("Iteration[1]"), NXOpen.CAE.Iteration)

        Dim iii As Integer = 1
        For Each resultType1 As CAE.ResultType in iteration1.GetResultTypes()

                If iii=12 Then
                        resultParameters1.SetGenericResultType(resultType1)
                        resultParameters1.MakeElementResult(False)

        resultParameters1.SetElementValueCriterion(NXOpen.CAE.Result.ElementValue
Criterion.Average)
                        Dim average2 As NXOpen.CAE.Result.Averaging = Nothing
                        average2.DoAveraging = True
                        average2.AverageAcrossPropertyIds = True
                        average2.AverageAcrossMaterialIds = True
                        average2.AverageAcrossElementTypes = True
                        average2.AverageAcrossFeatangle = True
                        average2.AverageAcrossAnglevalue = 45.0
                        average2.IncludeInternalElementContributions = True
                        resultParameters1.SetAveragingCriteria(average2)
                        Dim postviewId1 As Integer = Nothing
                        postviewId1 = theSession.Post.CreatePostviewForResult(0,
solutionResult1, False, resultParameters1)
                        Dim resultAccess1 As CAE.ResultAccess =
theSession.ResultManager.CreateResultAccess(results, resultParameters1)
                        Dim location as NXOpen.CAE.Result.Location
                        Dim NumEtr as integer = 5
                        Dim min as double()
                        Dim max as double()
                        Dim minID as integer()
                        Dim maxID as integer()
                        Dim minSubID as integer()
                        Dim maxSubID as integer()

        resultAccess1.AskNMinMaxLocation(NumEtr,location,min,max,minID,minSubID,m
axID,maxSubID)
                        Dim max1 As Double = resultAccess1.AskMaximum()
                        Dim index as integer = 0
                        Dim sum as double = 0
                        while index < NumEtr
                                sum = sum + max(index)
                                index+=1
                        End while
                        Dim mean as double =  sum/(NumEtr) ' Average peak contact
pressure calculation
                        file.WriteLine (Moment.ToString &" "&
forceInclinationAngle.ToString  &" "&  max1.ToString  &""&  mean.ToString) '
Saving value on a file
```

```
                End If
                iii+=1
        Next

        '----------------
        ' Display results
        '----------------
        Dim results2 As NXOpen.CAE.Result = CType(solresults, NXOpen.CAE.Result)
        Dim ii As Integer = 1
        For Each resultType4 As CAE.ResultType in iteration1.GetResultTypes()
                If ii=10 Then
                        Dim resultType5 As NXOpen.CAE.ResultType =
CType(iteration1.Find("ResultType[[Reaction Force][Nodal]]"),
NXOpen.CAE.ResultType)
                        resultParameters1.SetGenericResultType(resultType4)
                        resultParameters1.SetExcludeElementsNotVisible(False)
                        Dim postviewId4 As Integer = Nothing
                        postviewId4 = theSession.Post.CreatePostviewForResult(0,
solutionResult1, False, resultParameters1)
                        Dim resultAccess1 As CAE.ResultAccess =
theSession.ResultManager.CreateResultAccess(postviewId4)
                End If
                ii+=1
        Next
End While
file.Close()
Exit Sub
End Sub
End Module
        '
```

==========

References

[1] S. Arroyave-Tobón, G. Rao, and J.-M. Linares, "A multivariate statistical strategy to adjust musculoskeletal models," *J. Biomech.*, p. 109724, Mar. 2020, doi: 10.1016/j.jbiomech.2020.109724.

[2] B. Poncery, S. Arroyave-Tobón, E. Picault, and J.-M. Linares, "Effects of realistic sheep elbow kinematics in inverse dynamic simulation," *PLOS ONE*, vol. 14, no. 3, p. e0213100, Mar. 2019, doi: 10.1371/journal.pone.0213100.

[3] J. Becker, E. Mermoz, and J.-M. Linares, "Joint Loading Estimation Method for Horse Forelimb High Jerk Locomotion: Jumping," *J. Bionic Eng.*, vol. 16, no. 6, pp. 1143–1143, Nov. 2019, doi: 10.1007/s42235-019-0125-1.

[4] Anatomy & Physiology by OpenStax College, "OpenStaxCollege," 2013. .

[5] P. Egan, R. Sinko, P. R. LeDuc, and S. Keten, "The role of mechanics in biological and bio-inspired systems," *Nat. Commun.*, vol. 6, no. 1, Nov. 2015, doi: 10.1038/ncomms8418.

[6] X. Wei, Y. Tian, and A. Joneja, "A study on revolute joints in 3D-printed non-assembly mechanisms," *Rapid Prototyp. J.*, vol. 22, no. 6, pp. 901–933, Oct. 2016, doi: 10.1108/RPJ-10-2014-0146.

[7] A. Bruyas, F. Geiskopf, and P. Renaud, "Design and Modeling of a Large Amplitude Compliant Revolute Joint: The Helical Shape Compliant Joint," *J. Mech. Des.*, vol. 137, no. 8, Aug. 2015, doi: 10.1115/1.4030650.

[8] G. J. Tortora and B. Derrickson, *Principles of anatomy and physiology*. Hoboken: Wiley, 2014.

[9] D. R. Mason, K. S. Schulz, Y. Fujita, P. H. Kass, and S. M. Stover, "In vitro force mapping of normal canine humeroradial and humeroulnar joints," *Am. J. Vet. Res.*, vol. 66, no. 1, pp. 132–135, Jan. 2005, doi: 10.2460/ajvr.2005.66.132.

[10] J. G. Alcid, C. S. Ahmad, and T. Q. Lee, "Elbow anatomy and structural biomechanics," *Clin. Sports Med.*, vol. 23, no. 4, pp. 503–517, Oct. 2004, doi: 10.1016/j.csm.2004.06.008.

[11] J. . Sancho-Bru, A. Pérez-González, M. Vergara-Monedero, and D. Giurintano, "A 3-D dynamic model of human finger for studying free movements," *J. Biomech.*, vol. 34, no. 11, pp. 1491–1500, Nov. 2001, doi: 10.1016/S0021-9290(01)00106-3.

[12] T. L. Haut Donahue, M. L. Hull, M. M. Rashid, and C. R. Jacobs, "A Finite Element Model of the Human Knee Joint for the Study of Tibio-Femoral Contact," *J. Biomech. Eng.*, vol. 124, no. 3, pp. 273–280, Jun. 2002, doi: 10.1115/1.1470171.

[13] S. D. Masouros, A. M. J. Bull, and A. A. Amis, "(i) Biomechanics of the knee joint," *Orthop. Trauma*, vol. 24, no. 2, pp. 84–91, Apr. 2010, doi: 10.1016/j.mporth.2010.03.005.

[14] M. Adouni, A. Shirazi-Adl, and R. Shirazi, "Computational biodynamics of human knee joint in gait: From muscle forces to cartilage stresses," *J. Biomech.*, vol. 45, no. 12, pp. 2149–2156, Aug. 2012, doi: 10.1016/j.jbiomech.2012.05.040.

[15] W. Mesfar and A. Shirazi-Adl, "Biomechanics of the knee joint in flexion under various quadriceps forces," *The Knee*, vol. 12, no. 6, pp. 424–434, Dec. 2005, doi: 10.1016/j.knee.2005.03.004.

[16] A. N. Amirudin, S. Parasuraman, A. Kadirvel, M. K. A. A. Khan, and I. Elamvazuthi, "Biomechanics of Hip, Knee and Ankle Joint Loading during Ascent and Descent Walking," *Procedia Comput. Sci.*, vol. 42, pp. 336–344, 2014, doi: 10.1016/j.procs.2014.11.071.

[17] T. P. Andriacchi, P. L. Briant, S. L. Bevill, and S. Koo, “Rotational Changes at the Knee after ACL Injury Cause Cartilage Thinning:,” *Clin. Orthop.*, vol. 442, no. NA;, pp. 39–44, Jan. 2006, doi: 10.1097/01.blo.0000197079.26600.09.

[18] T. Miyazaki, “Dynamic load at baseline can predict radiographic disease progression in medial compartment knee osteoarthritis,” *Ann. Rheum. Dis.*, vol. 61, no. 7, pp. 617–622, Jul. 2002, doi: 10.1136/ard.61.7.617.

[19] *Nationa lInstitute of Arthritis and Muscoloskeletan and Skin Diseases*, Apr. 2017. https://www.niams.nih.gov/health-topics/arthritis/advanced (accessed Mar. 31, 2020).

[20] F. Russell, Y. Zhu, W. Hey, R. Vaidyanathan, and P. Ellison, “A biomimicking design for mechanical knee joints,” *Bioinspir. Biomim.*, vol. 13, no. 5, p. 056012, Aug. 2018, doi: 10.1088/1748-3190/aad39d.

[21] A. Sandholm, C. Schwartz, N. Pronost, M. de Zee, M. Voigt, and D. Thalmann, “Evaluation of a geometry-based knee joint compared to a planar knee joint,” *Vis. Comput.*, vol. 27, no. 2, pp. 161–171, Feb. 2011, doi: 10.1007/s00371-010-0538-7.

[22] S. Sathasivam and P. S. Walker, “Optimization of the bearing surface geometry of total knees,” *J. Biomech.*, vol. 27, no. 3, pp. 255–264, Mar. 1994, doi: 10.1016/0021-9290(94)90002-7.

[23] S. Au, M. Berniker, and H. Herr, “Powered ankle-foot prosthesis to assist level-ground and stair-descent gaits,” *Neural Netw.*, vol. 21, no. 4, pp. 654–666, May 2008, doi: 10.1016/j.neunet.2008.03.006.

[24] N. Prasad, A. Ali, and D. Stanley, “Total elbow arthroplasty for non-rheumatoid patients with a fracture of the distal humerus: a minimum ten-year follow-up,” *Bone Jt. J.*, vol. 98-B, no. 3, pp. 381–386, Mar. 2016, doi: 10.1302/0301-620X.98B3.35508.

[25] A. Cil, C. J. Veillette, J. Sanchez-Sotelo, and B. F. Morrey, “Linked Elbow Replacement: A Salvage Procedure for Distal Humeral Nonunion:,” *J. Bone Jt. Surg.-Am. Vol.*, vol. 90, no. 9, pp. 1939–1950, Sep. 2008, doi: 10.2106/JBJS.G.00690.

[26] K. Andersson, “Elbow-joint morphology as a guide to forearm function and foraging behaviour in mammalian carnivores,” *Zool. J. Linn. Soc.*, vol. 142, no. 1, pp. 91–104, Sep. 2004, doi: 10.1111/j.1096-3642.2004.00129.x.

[27] B. A. Patel, “The hominoid proximal radius: re-interpreting locomotor behaviors in early hominins,” *J. Hum. Evol.*, vol. 48, no. 4, pp. 415–432, Apr. 2005, doi: 10.1016/j.jhevol.2005.01.001.

[28] S. Fujiwara, “Olecranon orientation as an indicator of elbow joint angle in the stance phase, and estimation of forelimb posture in extinct quadruped animals,” *J. Morphol.*, vol. 270, no. 9, pp. 1107–1121, Sep. 2009, doi: 10.1002/jmor.10748.

[29] S. B. Boren, “3-D Morphometric Analysis of the Primate Elbow Joint,” University of Arkansas, Fayetteville, 2014.

[30] X. Wang, K. Kato, K. Adachi, and K. Aizawa, “Loads carrying capacity map for the surface texture design of SiC thrust bearing sliding in water,” *Tribol. Int.*, vol. 36, no. 3, pp. 189–197, Mar. 2003, doi: 10.1016/S0301-679X(02)00145-7.

[31] M. Fesanghary and M. M. Khonsari, “On the optimum groove shapes for load-carrying capacity enhancement in parallel flat surface bearings: Theory and experiment,” *Tribol. Int.*, vol. 67, pp. 254–262, Nov. 2013, doi: 10.1016/j.triboint.2013.08.001.

[32] M. Qiu and B. Raeymaekers, “The load-carrying capacity and friction coefficient of incompressible textured parallel slider bearings with surface roughness inside the texture

features," *Proc. Inst. Mech. Eng. Part J J. Eng. Tribol.*, vol. 229, no. 4, pp. 547–556, Apr. 2015, doi: 10.1177/1350650114545352.

[33] J.-R. Lin, "Optimal design of one-dimensional porous slider bearings using the Brinkman model," *Tribol. Int.*, vol. 34, no. 1, pp. 57–64, Jan. 2001, doi: 10.1016/S0301-679X(00)00138-9.

[34] L. Zamponi, E. Mermoz, J. M. Linares, and J. M. Sprauel, "Impact of geometrical defects on bearing assemblies with integrated raceways in aeronautical gearboxes," *Mech. Mach. Theory*, vol. 44, no. 6, pp. 1108–1120, Jun. 2009, doi: 10.1016/j.mechmachtheory.2008.10.005.

[35] R. Potočnik, P. Göncz, J. Flašker, and S. Glodež, "Fatigue life of double row slewing ball bearing with irregular geometry," *Procedia Eng.*, vol. 2, no. 1, pp. 1877–1886, Apr. 2010, doi: 10.1016/j.proeng.2010.03.202.

[36] S. Zupan and I. Prebil, "Carrying angle and carrying capacity of a large single row ball bearing as a function of geometry parameters of the rolling contact and the supporting structure stiffness," *Mech. Mach. Theory*, vol. 36, no. 10, pp. 1087–1103, Oct. 2001, doi: 10.1016/S0094-114X(01)00044-1.

[37] C. I. Papadopoulos, E. E. Efstathiou, P. G. Nikolakopoulos, and L. Kaiktsis, "Geometry Optimization of Textured Three-Dimensional Micro- Thrust Bearings," *J. Tribol.*, vol. 133, no. 4, Oct. 2011, doi: 10.1115/1.4004990.

[38] E. Dragoni, "Optimal design of radial cylindrical roller bearings for maximum load-carrying capacity," *Proc. Inst. Mech. Eng. Part C J. Mech. Eng. Sci.*, vol. 227, no. 11, pp. 2393–2401, Nov. 2013, doi: 10.1177/0954406213477579.

[39] S. Boedo and S. L. Eshkabilov, "Optimal Shape Design of Steadily Loaded Journal Bearings using Genetic Algorithms," *Tribol. Trans.*, vol. 46, no. 1, pp. 134–143, Jan. 2003, doi: 10.1080/10402000308982610.

[40] A. Gherca, A. Fatu, M. Hajjam, and P. Maspeyrot, "Influence of Surface Geometry on the Hydrodynamic Performances of Parallel Bearings in Transient Flow Conditions," *Tribol. Trans.*, vol. 56, no. 6, pp. 953–967, Nov. 2013, doi: 10.1080/10402004.2013.813997.

[41] A. Rezaei, W. Van Paepegem, P. De Baets, W. Ost, and J. Degrieck, "Adaptive finite element simulation of wear evolution in radial sliding bearings," *Wear*, vol. 296, no. 1–2, pp. 660–671, Aug. 2012, doi: 10.1016/j.wear.2012.08.013.

[42] W. Xiang, S. Yan, and J. Wu, "A comprehensive method for joint wear prediction in planar mechanical systems with clearances considering complex contact conditions," *Sci. China Technol. Sci.*, vol. 58, no. 1, pp. 86–96, Jan. 2015, doi: 10.1007/s11431-014-5685-z.

[43] S. S. Goilkar and H. Hirani, "Design and Development of a Test Setup for Online Wear Monitoring of Mechanical Face Seals Using a Torque Sensor," *Tribol. Trans.*, vol. 52, no. 1, pp. 47–58, Dec. 2008, doi: 10.1080/10402000802163017.

[44] E. Mermoz, D. Fages, L. Zamponi, J.-M. Linares, and J.-M. Sprauel, "New methodology to define roller geometry on power bearings," *CIRP Ann.*, vol. 65, no. 1, pp. 157–160, 2016, doi: 10.1016/j.cirp.2016.04.095.

[45] E. A. Muyderman, "BEARINGS," *Sci. Am.*, vol. 214, no. 3, pp. 60–73, 1966.

[46] M. A. Hili, T. Fakhfakh, L. Hammami, and M. Haddar, "Shaft misalignment effect on bearings dynamical behavior," *Int. J. Adv. Manuf. Technol.*, vol. 26, no. 5–6, pp. 615–622, Sep. 2005, doi: 10.1007/s00170-004-2013-y.

[47] N. B. Messaoud, S. Bouaziz, T. Fakhfakh, M. Maatar, and M. Haddar, "Dynamic behavior of active magnetic bearings in presence of angular misalignment defect," *Int. J. Appl. Mech.*, vol. 03, no. 03, pp. 491–505, Sep. 2011, doi: 10.1142/S1758825111001093.

[48] Q. Zhang, C. Hua, and G. Xu, “A mixture Weibull proportional hazard model for mechanical system failure prediction utilising lifetime and monitoring data,” *Mech. Syst. Signal Process.*, vol. 43, no. 1–2, pp. 103–112, Feb. 2014, doi: 10.1016/j.ymssp.2013.10.013.

[49] D. Siegel, C. Ly, and J. Lee, “Methodology and Framework for Predicting Helicopter Rolling Element Bearing Failure,” *IEEE Trans. Reliab.*, vol. 61, no. 4, pp. 846–857, Dec. 2012, doi: 10.1109/TR.2012.2220697.

[50] J. V. Poplawski, S. M. Peters, and E. V. Zaretsky, “Effect Of Roller Profile On Cylindrical Roller Bearing Life Prediction—Part I: Comparison of Bearing Life Theories,” *Tribol. Trans.*, vol. 44, no. 3, pp. 339–350, Jan. 2001, doi: 10.1080/10402000108982466.

[51] Y. Feng, X. Huang, J. Chen, H. Wang, and R. Hong, “Reliability-based residual life prediction of large-size low-speed slewing bearings,” *Mech. Mach. Theory*, vol. 81, pp. 94–106, Nov. 2014, doi: 10.1016/j.mechmachtheory.2014.06.013.

[52] H.-T. Lin, G. G. Leisk, and B. Trimmer, “GoQBot: a caterpillar-inspired soft-bodied rolling robot,” *Bioinspir. Biomim.*, vol. 6, no. 2, p. 026007, Jun. 2011, doi: 10.1088/1748-3182/6/2/026007.

[53] S. Kim, C. Laschi, and B. Trimmer, “Soft robotics: a bioinspired evolution in robotics,” *Trends Biotechnol.*, vol. 31, no. 5, pp. 287–294, May 2013, doi: 10.1016/j.tibtech.2013.03.002.

[54] F. Boyer and M. Porez, “Multibody system dynamics for bio-inspired locomotion: from geometric structures to computational aspects,” *Bioinspir. Biomim.*, vol. 10, no. 2, p. 025007, Mar. 2015, doi: 10.1088/1748-3190/10/2/025007.

[55] H. Zhou *et al.*, “Bio-inspired flow sensing and prediction for fish-like undulating locomotion: A CFD-aided approach,” *J. Bionic Eng.*, vol. 12, no. 3, pp. 406–417, Sep. 2015, doi: 10.1016/S1672-6529(14)60132-3.

[56] S. Lohmeier, T. Buschmann, H. Ulbrich, and F. Pfeiffer, “Modular joint design for performance enhanced humanoid robot LOLA,” in *Proceedings 2006 IEEE International Conference on Robotics and Automation, 2006. ICRA 2006.*, Orlando, FL, USA, 2006, pp. 88–93, doi: 10.1109/ROBOT.2006.1641166.

[57] C. Audibert, J. Chaves-Jacob, J.-M. Linares, and Q.-A. Lopez, “Bio-inspired method based on bone architecture to optimize the structure of mechanical workspieces,” *Mater. Des.*, vol. 160, pp. 708–717, Dec. 2018, doi: 10.1016/j.matdes.2018.10.013.

[58] V. K. Goel, D. Singh, and V. Bijlani, “Contact Areas in Human Elbow Joints,” *J. Biomech. Eng.*, vol. 104, no. 3, pp. 169–175, Aug. 1982, doi: 10.1115/1.3138344.

[59] “NX Siemens.” www.plm.automation.siemens.com (Section produits NX).

[60] K. Yang, G. Zhang, Y. W. Wang, and S. Cai, “Finite element analysis on contact stress of high-speed railway bearings,” *IOP Conf. Ser. Mater. Sci. Eng.*, vol. 504, p. 012073, Apr. 2019, doi: 10.1088/1757-899X/504/1/012073.

[61] S. A. Maas, B. J. Ellis, D. S. Rawlins, and J. A. Weiss, “Finite element simulation of articular contact mechanics with quadratic tetrahedral elements,” *J. Biomech.*, vol. 49, no. 5, pp. 659–667, Mar. 2016, doi: 10.1016/j.jbiomech.2016.01.024.

[62] R. Willing, G. J. W. King, and J. A. Johnson, “The effect of implant design of linked total elbow arthroplasty on stability and stress: a finite element analysis,” *Comput. Methods Biomech. Biomed. Engin.*, vol. 17, no. 11, pp. 1165–1172, Aug. 2014, doi: 10.1080/10255842.2012.739161.

[63] E. Ayhan and Ç. Ayhan, “Kinesiology of the elbow complex,” in *Comparative Kinesiology of the Human Body*, Elsevier, 2020, pp. 191–210.